Research Activities

– Synchrotron Radiation Experiments –

Temperature dependence of the coupling parameter in the strange metal state of heavily overdoped cuprate superconductor

Y. Miyai[a], S. Ideta[b], M. Arita[b], K. Tanaka[c], M. Oda[d], T. Kurosawa[e] and K. Shimada[b,f,g]

[a]*Department of Applied Physics, KTH Royal Institute of Technology, Stockholm, 106-91, Sweden*
[b] *Hiroshima Synchrotron Radiation Center, Hiroshima University, Higashi-Hiroshima 739-8526, Japan*
[c] *UVSOR-III Synchrotron, Institute for Molecular Science, Okazaki 444-8585, Japan*
[d] *Department of Physics, Hokkaido University, Sapporo 060-0809, Japan*
[e] *Faculty of Science and Engineering, Muroran Institute of Technology, Muroran 050-8585, Japan*
[e] *Research Institute for Semiconductor Engineering (RISE), Hiroshima University, Higashi-Hiroshima 739-8527, Japan*
[g] *The International Institute for Sustainability with Knotted Chiral Meta Matter (WPI-SKCM^2), Hiroshima University, Higashi-Hiroshima 739-8526, Japan*

Keywords: High-T_c superconductor, ARPES

Since the discovery of high-transition-temperature (T_c) superconductivity in cuprates, unusual physical properties such as metal-insulator transition [1], pseudogap state, spin and charge ordering [2,3] in the underdoped to the optimally-doped region have attracted much interest. There have been extensive studies to elucidate their correlation to the mechanism of the high-T_c. In contrast, the electronic states in the heavily overdoped region have been regarded as the Fermi liquid. However, non-Fermi liquid like behaviors such as the strange metal state [4], ferromagnetic fluctuation [5], and charge order [6], have been discovered in the overdoped region, renewing scientific interests of cuprate superconductors.

These physical properties arise from many-body interactions involving the complex entanglement of internal degrees of freedom such as spin, charge, lattice, and orbital. In this study, we performed quantitative lineshape analyses of angle-resolved photoemission spectroscopy (ARPES) spectra to evaluate the self-energy, which reflects information about many-body interactions through its functional form. We have revealed distinct energy scales in the self-energy, namely, the low-energy kink (LEK) and the high-energy anomaly (HEA) in heavily overdoped Bi-based high-temperature cuprates, $(Bi,Pb)_2Sr_2CuO_{6+\delta}$ (Pb-Bi2201) [7].

We experimentally extracted the self-energy (Σ_{tot}) based on the Kramers-Kronigh relation. By introducing the model function, we successfully reproduced the self-energy responsible for the HEA (Σ_{HEA}) and extracted the self-energy responsible for the LEK (Σ_{LEK}) by subtracting Σ_{HEA} from Σ_{tot}. Figure 1(b) shows the temperature dependence of the coupling parameter, $\lambda(T)$, determined from the gradient of the real part of the self-energy at the Fermi level in Fig.1(a). One can see that $\lambda_{\mathrm{tot}} \sim 1$ at 300 K, indicating that the normal state is strongly correlated. Since Σ_{HEA} is dominant at 300 K, Σ_{HEA} should correspond to the self-energy in the strange metal state. On the other hand, we found that $\lambda_{\mathrm{LEK}}(T) = \lambda_{\mathrm{tot}}(T) - \lambda_{\mathrm{HEA}}$ deviates from the theoretical calculation based on the temperature-independent Eliashberg function of the electron-phonon interaction [8], revealing that the LEK is remarkably enhanced at low temperatures. It suggests an unexplored mechanism to enhance the coupling parameter emerging from entangled many-body interactions. Our results give insight into the unusual strange metal state as well as the origin of the exotic

superconductivity in cuprates.

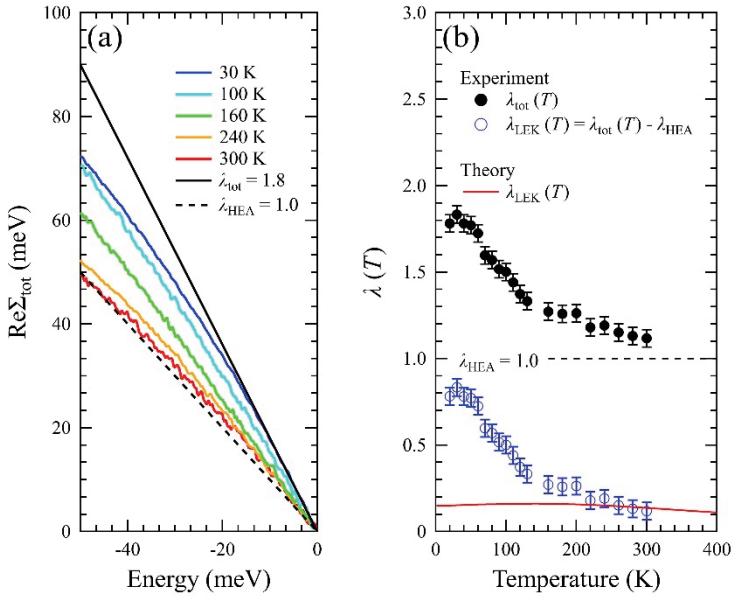

Figure 1 (a) The real part of the self-energy, $\mathrm{Re}\Sigma_{\mathrm{tot}}(\omega)$, for some representative temperatures. Black solid line indicates the magnitude of the coupling parameter calculated from $\mathrm{Re}\Sigma_{\mathrm{tot}}(\omega)$ at 300 K, while the black dashed line corresponds to the real part of the model self-energy for HEA, $\mathrm{Re}\Sigma_{\mathrm{HEA}}(\omega)$. (b) The temperature dependence of the coupling parameter. Black and blue dots indicate the total coupling parameter, $\lambda_{\mathrm{tot}}(T)$, and the coupling parameter for the LEK, $\lambda_{\mathrm{LEK}}(T) = \lambda_{\mathrm{tot}}(T) - \lambda_{\mathrm{HEA}}$, respectively, where λ_{HEA} denotes the coupling parameter for the HEA (black dashed line). The red curve shows the theoretical temperature dependence of the coupling parameter for LEK using the Eliashberg function in Ref. [8].

1. M. Imada *et al*., *Reviews of Modern Physics* **70**, 1039 (1998).
2. A. Damascelli *et al*., *Reviews of Modern Physics* **75**, 473 (2003).
3. J. A. Sobota *et al., Reviews of Modern Physics* **93**, 025006 (2021).
4. J. Ayres *et al*., *Nature* **595**, 661-666 (2021).
5. K. Kurashima *et al*., *Physical Review Letters* **121**, 057002 (2018).
6. Y. Y. Peng *et al*., *Nature Materials* **17**, 697 (2018).
7. Y. Miyai, *et al*., *Physical Review Research* **7**, L012039 (2025).
8. W. Meeasana, *et al*., *Physical Review Letters* **96**, 157003 (2006).

Electronic States in Superconducting Type-II Dirac Semimetal: 1T-Pdsete

Yogendra Kumar[1], Shiv Kumar[2], Venkateswara Yenugonda[3,4], Ryohei Oishi[1], Jayita Nayak[4], Chaoyu Chen[5], Ravi Prakash Singh[6], Takahiro Onimaru[1], Yasuyuki Shimura[1], Shin-ichiro Ideta[2], and Kenya Shimada[2,7,8],

[1]*Graduate School of Advanced Science and Engineering, Hiroshima University, Higashi-Hiroshima 739-8526, Japan*

[2]*Research Institute for Synchrotron Radiation Science (HiSOR), Hiroshima University, Higashi-Hiroshima 739-0046, Japan*

[3]*Department of Physics, SUNY Buffalo State University, Buffalo, New York 14222, USA*

[4]*Department of Physics, Indian Institute of Technology, Kanpur 208016, India*

[5]*Songshan Lake Materials Laboratory, Dongguan 523808, China*

[6]*Department of Physics, Indian Institute of Science Education and Research, Bhopal 462066, India*

[7]*The International Institute for Sustainability with Knotted Chiral Meta Matter (WPI-SKCM^2), Hiroshima University, Higashi-Hiroshima 739-8526, Japan*

[8]*Research Institute for Semiconductor Engineering (RISE), Hiroshima University, Higashi-Hiroshima 739-8527, Japan*

Keywords: Topological semimetal (Dirac/Weyl), Surface states, superconductivity, DFT.

Topological semimetals, like Dirac, Weyl, and topological nodal-line semimetals, have drawn significant theoretical and experimental interest due to their distinct band crossing forms, degeneracies, and spin textures near the Fermi level (E_F) [1,2,3,4]. Weyl semimetals emerge from Dirac semimetals when either spatial inversion symmetry or time-reversal symmetry is broken [5], hosting massless chiral fermions in the bulk that behave like magnetic monopoles in momentum space and give rise to discontinuous Fermi arcs in the topological surface states. These systems exhibit remarkable properties, such as high carrier mobility and large negative magnetoresistance, often discussed in the context of the Adler–Bell–Jackiw anomaly describing chiral current nonconservation in gauge fields [6]. They are classified into type-I, preserving Lorentz symmetry (e.g., TaAs), and type-II, lacking Lorentz symmetry (e.g., WTe_2, $MoTe_2$). The latter shows anisotropic chiral anomalies leading to anisotropic magnetotransport [4,7]. Within this context, 1T-$PdTe_2$ has gained significant attention as a type-II Dirac semimetal in addition to superconductivity [8–10]. Furthermore, 1T-$PdTe_2$ has several tilted Dirac points in the bulk along the Γ–A direction of the bulk Brillouin zone. These Dirac points are protected by the strong spin-orbit interaction because the symmetry of the $R^{+}_{5,6}$ states with $J = 3/2$ (at the Γ point) derived from Te $5p_x$, $5p_y$ orbitals cannot hybridize with the R^{-}_{4} state with $J = 1/2$ (at the Γ point) derived from Te $5pz$ orbital due to different J values [11]. Moreover, 1T-$PdTe_2$ hosts several topological surface states (TSSs) in bulk band gaps with inverted parity [10,11], which remain robust against perturbations that preserve topological invariants and can give rise to exotic quantum phenomena, including high-mobility transport, the quantum spin Hall effect [12], the quantum anomalous Hall effect [13], and possibly the emergence of Majorana fermions in the superconducting state [14], and magnetic monopole-like excitations [15].

To transform 1T-$PdTe_2$ into a Weyl semimetal, one can either break time-reversal symmetry by introducing magnetic elements or break inversion symmetry through lattice modification [16]. In particular, replacing one Te layer in 1T-$PdTe_2$ completely with a Se layer has been proposed to remove the inversion symmetry point, with DFT calculations confirming a lifting of band degeneracy near the zone boundary [11]. Experimentally, 1T-PdSeTe exhibits a superconducting transition temperature of $T_c = 2.74$ K, about 1.7 times higher than that of 1T-$PdTe_2$ ($T_c = 1.64$ K) [8,17]. Magnetic susceptibility and heat capacity measurements have shown type-II superconductivity with strong anisotropy, but only a 20% superconducting volume fraction [8]. The enhancement in T_c has been attributed to a combination of chemical pressure and defects/disorder effects [8]. However, there has been no direct investigation into the surface and bulk electronic structure of bulk 1T-PdSeTe so far.

In order to investigate the electronic band structure of 1T-PdSeTe, we have carried out angle-resolved photoemission spectroscopy (ARPES) measurements at linear undulator beamline BL-1 of the Research

Institute of Synchrotron Radiation Science (HiSOR), Hiroshima University. We cut the small pieces of single crystal from the large single crystal and mounted them on the sample holder of BL-1. We used the post-cleaving method to get the fresh, new, and flat surface required for ARPES. To check different termination cleaving possibilities, we cleaved many samples, and no difference was found in the band structure.

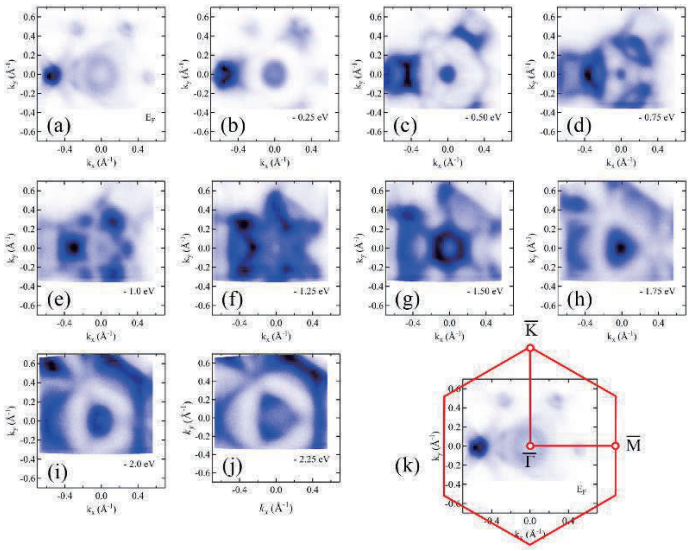

FIGURE 1. [(a)–(j)] Constant energy contour from the E_F down to -2.25 eV measured at $h\nu$ = 25 eV. Here, k_x and $_ky$ directions are parallel to $\bar{\Gamma}-\bar{M}$ direction and $\bar{\Gamma}-\bar{K}$ direction, respectively. The bottom of the electronlike band centered at the Γ point exists at the energy of -0.75 eV. The Dirac point of the topological surface state exists at the $\bar{\Gamma}$ point at the energy of -1.75 eV. (k) The first Brillouin zone overlaid on (a).

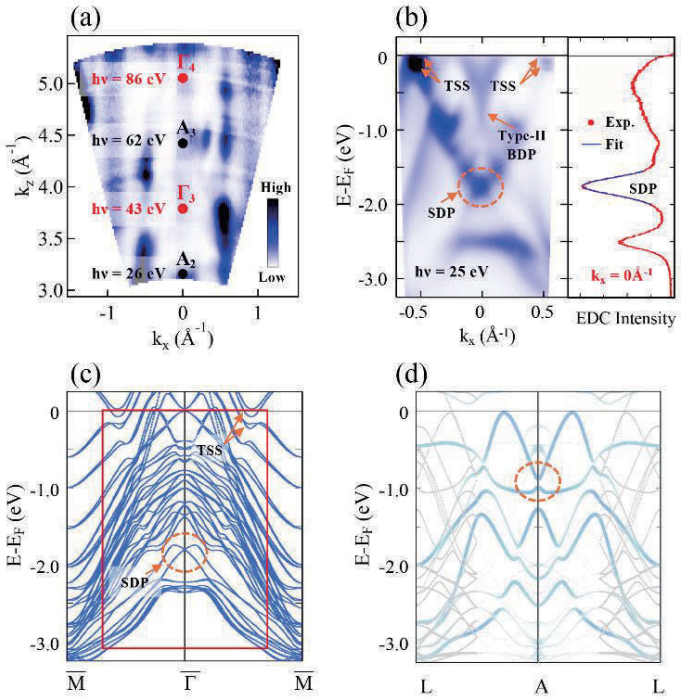

FIGURE 2. (a) Fermi surface cross section of PdSeTe by the k_x-k_z plane. Here k_x and k_z directions are parallel to $\bar{\Gamma}-\bar{M}$ direction and Γ–A direction, respectively. High symmetry points (A_2, Γ_3, A_3, and Γ_4) and required photon energies to reach these points are shown. (b) ARPES intensity plot near the L–A–L direction (left panel) and energy distribution curve (EDC) along kx = 0Å-1 (right panel) taken at $h\nu$ = 25 eV. The dashed circle shows the surface-derived Dirac point (SDP), and arrows show the topological surface states (TSS) and bulk-derived type-II Dirac point (BDP). The blue line in the right panel shows a Lorentzian fit. (c) The DFT calculation result for 5 ML along the $\bar{M}-\bar{\Gamma}-\bar{M}$ high-symmetry direction. The red box corresponds to the range of the ARPES image in (b). The SDP and TSS corresponding to those in (b) are also shown. (d) The DFT calculation result of the bulk band dispersion along L–A–L direction obtained from a supercell with disordered Se and Te atoms. The degeneracy of the BDP is lifted just at the A point (see dashed circle part). However, the BDP exists along the Γ-A direction, closer to the A point.

We have mapped out the Fermi surface at different photon energies; Figs. 1 show constant energy mapping from the E_F down to -2.25 eV taken at hν = 25 eV. Photon energy-dependent measurements were also carried out from 25 eV to 100 eV as shown in Fig. 2(a), and the inner potential was determined based on the weak but finite k_z periodicity of several bands. Fig. 2(b) shows the ARPES intensity map taken at hν=25 eV, near the A point of the bulk Brillouin zone. By comparing the results of slab calculation in Fig. 2(c) as well as bulk band calculation in Fig. 2(d), surface and bulk-derived bands are identified. The results were published in the Physical Review Research **7**, 013174 (2025).

REFERENCES

1. M. Z. Hasan and C. L. Kane, *Colloquium:* Topological insulators, Rev. Mod. Phys. **82**, 3045 (2010).
2. M. Neupane, S.-Y. Xu, R. Sankar, N. Alidoust, G. Bian, C. Liu, I. Belopolski, T.-R. Chang, H.-T. Jeng, H. Lin, A. Bansil, F. Chou, and M. Z. Hasan, Observation of a three-dimensional topological Dirac semimetal phase in high-mobility Cd3As2, Nat. Commun. **5**, 3786 (2014).
3. B. Yan and C. Felser, Topological materials: Weyl semimetals, Annu. Rev. Condens. Matter Phys. **8**, 337 (2017).
4. B. Q. Lv, T. Qian, and H. Ding, Experimental perspective on three-dimensional topological semimetals, Rev. Mod. Phys. **93**, 025002 (2021).
5. X. Wan, A. M. Turner, A. Vishwanath, and S. Y. Savrasov, Topological semimetal and Fermi-arc surface states in the electronic structure of pyrochlore iridates, Phys. Rev. B: Condens. Matter Mater. Phys. **83**, 205101 (2011).
6. H. B. Nielsen and M. Ninomiya, The Adler-Bell-Jackiw anomaly and Weyl fermions in a crystal, Phys. Lett. B **130**, 389 (1983).
7. T. Nag and S. Nandy, Magneto-transport phenomena of type-I multi-Weyl semimetals in co-planar setups, J. Phys.: Condens. Matter **33**, 075504 (2021).
8. W. Liu, S. Li, H. Wu, N. Dhale, P. Koirala, and B. Lv, Enhanced superconductivity in the Se-substituted 1T-PdTe2, Phys. Rev. Mater. **5**, 014802 (2021).
9. J. Cook, S. Mardanya, Q. Lu, C. Conner, M. Snyder, X. Zhang, J. McMillen, G. Watson, T.-R. Chang, and G. Bian, Observation of gapped topological surface states and isolated surface resonances in PdTe2 ultrathin films, Nano Lett. **23**, 1752 (2023).
10. O. J. Clark, M. J. Neat, K. Okawa, L. Bawden, I. Markovic, F. ´ Mazzola, J. Feng, V. Sunko, J. M. Riley, W. Meevasana, J. Fujii, I. Vobornik, T. K. Kim, M. Hoesch, T. Sasagawa, P. Wahl, M. S. Bahramy, and P. D. C. King, Fermiology and superconductivity of topological surface states in PdTe2, Phys. Rev. Lett. **120**, 156401 (2018).
11. M. S. Bahramy, O. J. Clark, B. J. Yang, J. Feng, L. Bawden, J. M. Riley, I. Markovic, F. Mazzola, V. Sunko, D. Biswas, S. P. Cooil, M. Jorge, J. W. Wells, M. Leandersson, T. Balasubramanian, J. Fujii, I. Vobornik, J. E. Rault, T. K. Kim, M. Hoesch *et al.*, Ubiquitous formation of bulk Dirac cones and topological surface states from a single orbital manifold in transition-metal dichalcogenides, Nat. Mater. **17**, 21 (2018).
12. B. A. Bernevig, T. L. Hughes, and S.-C. Zhang, Quantum spin Hall effect and topological phase transition in HgTe quantum wells, Science **314**, 1757 (2006).
13. R. Yu, W. Zhang, H.-J. Zhang, S.-C. Zhang, X. Dai, and Z. Fang, Quantized anomalous Hall effect in magnetic topological insulators, Science **329**, 61 (2010).
14. L. Fu and E. Berg, Odd-parity topological superconductors: Theory and application to Cu*x*Bi2Se3, Phys. Rev. Lett. **105**, 097001 (2010).
15. X.-L. Qi, R. Li, J. Zang, and S.-C. Zhang, Inducing a magnetic monopole with topological surface states, Science **323**, 1184 (2009).
16. R. Xiao, C. Cheung, P. Gong, W. Lu, J. Si, and Y. Sun, Inversion symmetry breaking induced triply degenerate points in orderly arranged PtSeTe family materials, J. Phys.: Condens. Matter **30**, 245502 (2018).
17. W. Liu, M. R. Osanloo, X. Wang, S. Li, N. Dhale, H. Wu, M. L. Van de Put, S. Tiwari, W. G. Vandenberghe, and B. Lv, New Verbeekite-type polymorphic phase and rich phase diagram in the $PdSe_{2-x}Te_x$ system, Phys. Rev. B **104**, 024507 (2021).

Fermi surface mapping of the surface electronic structure of antiferromagnet NdBi

R. Yamamoto[a,b], Y. Nishioka[c], K. Ideura[c], M. Arita[d], S. Ideta[d], K. Shimda[a,d,e], A. Kimura[a,c,e], T. Onimaru[c], and K. Kuroda[a,c,e]

[a] *International Institute for Sustainability with Knotted Chiral Meta Matter (WPI-SKCM²), Hiroshima University, Japan*
[b] *Max Planck Institute for Chemical Physics of Solids, Dresden, Germany*
[c] *Graduate School of Advanced Science and Engineering, Hiroshima University, Japan*
[d] *HiSOR, Hiroshima University, Japan*
[e] *Research Institute for Semiconductor Engineering, Hiroshima University, Japan*

Keywords: antiferromagnetism, spin splitting, band structures, ARPES.

In recent years, antiferromagnets have attracted growing attention as a new platform for studying spin-polarized electrons [1, 2]. Unlike ferromagnets, antiferromagnetic (AFM) materials can exhibit spin splitting even in the absence of net magnetization, due to either time-reversal (*T*) or inversion (*P*) symmetry breaking. This phenomenon can be understood from the perspectives of magnetic multipoles [3] and altermagnetism [4]. The emergence of spin-split electronic structures in AFM states has been intensively investigated [5–7]. Furthermore, the AFM order parameter, such as the Néel vector, can function as a state variable for controlling these properties. However, the field of AFM spintronics is still in its early stages, and the difficulty in directly observing spin splitting in AFM states hampers our understanding of how AFM order affects the electronic structure.

Rare-earth monopnictides RX (R: rare-earth, X: pnictogen), which crystallize in a NaCl-type structure, have recently gained renewed interest because their electronic structures can be significantly altered by AFM ordering. Angle-resolved photoemission spectroscopy (ARPES) has revealed both the sensitivity of their band structures to AFM configurations and the strong coupling between itinerant carriers and localized 4*f* electrons [8, 9]. In particular, NdBi exhibits the emergence of surface states and the development of band splitting across the AFM transition at T_N=24 K [10]. Density functional theory (DFT) calculations have suggested that this originates from spin-split surface states formed within a band-folding-induced hybridization gap [11]. So far, the spin information of these states has been inferred only through circular dichroism (CD) in ARPES measurements [10], although CD primarily probes orbital, rather than spin, degrees of freedom. Therefore, spin-resolved ARPES (spin-ARPES) is essential for reliably determining the spin splitting and its momentum-space texture.

NdBi exhibits an AFM type-I structure [12] and, therefore, multiple magnetic domains may exist as in isostructural compounds. Accordingly, it is essential to account for domain distributions and to distinguish between different domains in ARPES and spin-ARPES experiments. In this work, we employed synchrotron-radiation ARPES at HiSOR and polarization microscopy to determine the electronic band structure of NdBi in the AFM phase.

Figures 1(a) and 1(b) show polarized optical microscope images of the cleaved (001) surface in the paramagnetic (PM) and AFM states. The image contrast changes across T_N, likely originating from the birefringence effect due to the tetragonal magnetic structure [8, 9]. The spatial distribution of the domains becomes apparent in Fig. 1(c), which was obtained by subtracting the images taken above and below T_N. Notably, the domain size was large enough

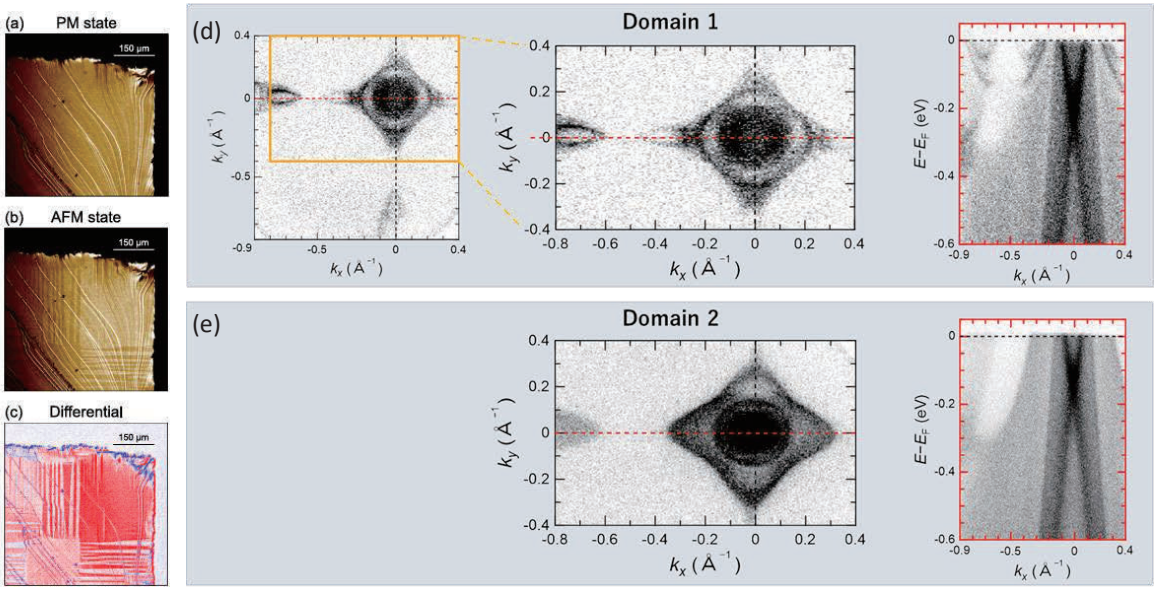

Fig. 1: . (a), (b) Polarized microscope images of the cleaved (001) surface of NdBi in PM and AFM states. (c) The differential intensity image is obtained by subtracting the intensity between images of (a) and (b). (d) and (e) Fermi surface maps and the correspoinding energy dispersion of the surface state below T_N acquired at diffferent magneti domains.

to resolve the AFM domains by synchrotron-radiation ARPES and laser spin-ARPES system [13].

Figure 1(d) shows the Fermi surface obtained by synchrotron-based ARPES in the AFM state. Below T_N, surface bands were clearly observed along the kx axis but not along the ky axis. The observed C_2-symmetric anisotropic electronic structure is consistent with a previous report [43] indicating that the magnetic moments are aligned within the cleaved plane, as well as with the emergence of birefringence observed via polarization microscopy. Therefore, the observed C_2-symmetric electronic structure is considered to reflect the intrinsic electronic structure of NdBi, revealed by selectively probing spatially distributed AFM domains. Supporting this interpretation, when the measurement position on the sample was changed, the surface bands disappeared and a different Fermi surface shape was observed [Fig. 1(e)]. This work has been published in Physical Review Research [14].

References

[1] T. Jungwirth, X. Marti, P. Wadley, and J. Wunderlich, Nature Nanotech. **11**, 231 (2016).
[2] V. Baltz *et al*., Rev. Mod. Phys. **90**, 015005 (2018).
[3] H. Watanabe and Y. Yanase, Phys. Rev. B **98**, 245129 (2018).
[4] L. Šmejkal, J. Sinova, and T. Jungwirth, Phys. Rev. X **12**, 040501 (2022).
[5] Y.-P. Zhu et al, Nature (London) **626**, 523 (2024).
[6] J. Krempaský *et al*., Nature (London) **626**, 517 (2024).
[7] T. Osumi *et al.*, Phys. Rev. B **109**, 115102 (2024).
[8] K. Kuroda *et al.*, Nature Commun. **11**, 2888 (2020).
[9] Y. Arai *et al*, Nature Mater. **21**, 410 (2022).
[10] B. Schrunk *et al*., Nature (London) **603**, 610 (2022).s
[11] L.-L. Wang *et al.*, Commun. Phys. **6**, 78 (2023).
[12] T. Tsuchida and W. E. Wallace, J. Chem. Phys. **43**, 2087 (1965).
[13] T. Iwata *et al.*, Sci. Rep. **14**, 127 (2024).
[14] R. Yamamoto *et al.*, Phys. Rev. Research **7**, L022005 (2025).

High resolution ARPES study of type Ⅳ Dirac band structures in SrAgBi

Di Wu[a], Yudai Miyai[b,c], Shin-ichiro Ideta[b], Shilong Wu[a,d]

[a]*Institute of Physics, Chinese Academy of Sciences*
[b]*Research Institute for Synchrotron Radiation Science, Hiroshima University*
[c]*Department of Physical Science, Graduate School of Science, Hiroshima University*
[d]*Songshan Lake Materials Laboratory*

Keywords: Topological semimetals, type Ⅳ Dirac cone, ARPES, Dresselhaus spin splitting.

In high-energy physics, relativistic massless Weyl and Dirac fermions exhibit isotropic linear dispersion relations to preserve Poincaré symmetry. Condensed matter systems, however, can host emergent fermionic excitations without high-energy analogues. We report a predicted nonlinear Dirac fermion in SrAgBi semimetal-distinct from known high-energy counterparts-designated as a type-IV Dirac fermion. This novel quasiparticle features a nonlinear dispersion relationship and shares characteristics with type-II Dirac fermions, particularly in constituting by both electron and hole pockets. Notably, a type-II Dirac fermion coexists adjacent to this new fermion, suggesting the first experimental observation of type-II/type-IV Dirac fermion coexistence and interaction in SrAgBi [1]. Given the current absence of direct ARPES evidence for the exotic Dirac fermion, we conducted high-resolution ARPES measurements on this compound.

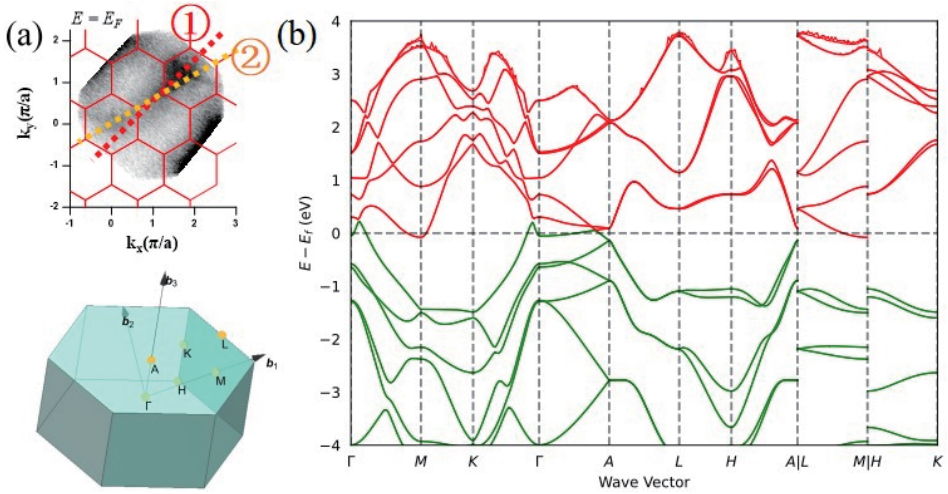

FIGURE 1. (**a)** Schematic graph of the 3D Brillouin zone and Fermi surface of the SrAgBi measured with 60 eV, with the red and yellow lines showing the directions where the band dispersion spectra in Fig 2 and 3 are measured. (**b**) the DFT calculations of SrAgBi.

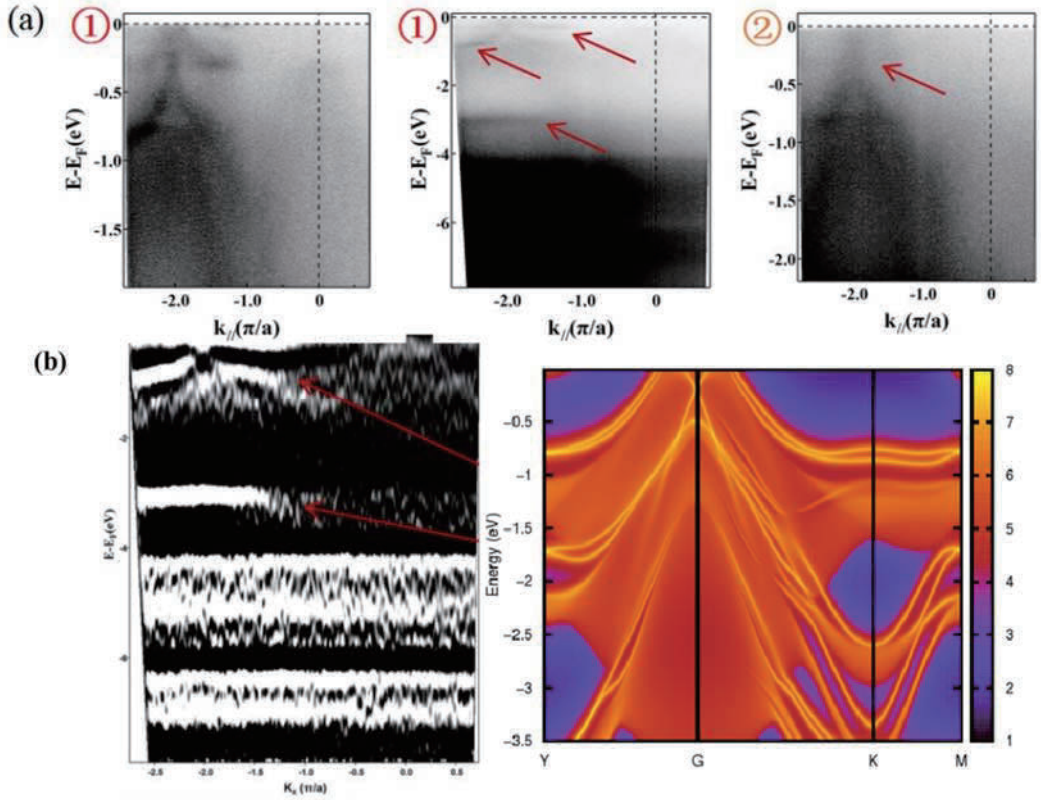

FIGURE 2. **(a)** Band dispersion spectra near both “1” and “2” lines, red arrows denote the flat bands; **(b)** Red arrows indicate the pair of bands showing hidden Dresselhaus SOC splitting, the large energy range dispersion spectra derived from ARPES experiments and its corresponding second derivative spectrum along Γ-K direction. The right panel shows the DFT calculations of SrAgBi of both bulk and surface states.

In BL-1 endstation of HiSOR, we conducted high-resolution angle-resolved photoemission spectroscopy (ARPES) measurements on SrAgBi. Firstly, a predicted Dirac semimetal candidate SrAgBi single crystal was confirmed by integrated photoemission. The results of angular-integrated photoemission spectra—not depicted here—reveals distinct characteristic peaks arising from the core levels of Sr, Ag, and Bi elements. This study specifically targeted the Type-IV Dirac cone band at point A and the Dresselhaus-type band splitting at point H; the latter originates from local inversion symmetry breaking induced by the D_{3h} point group symmetry [2].

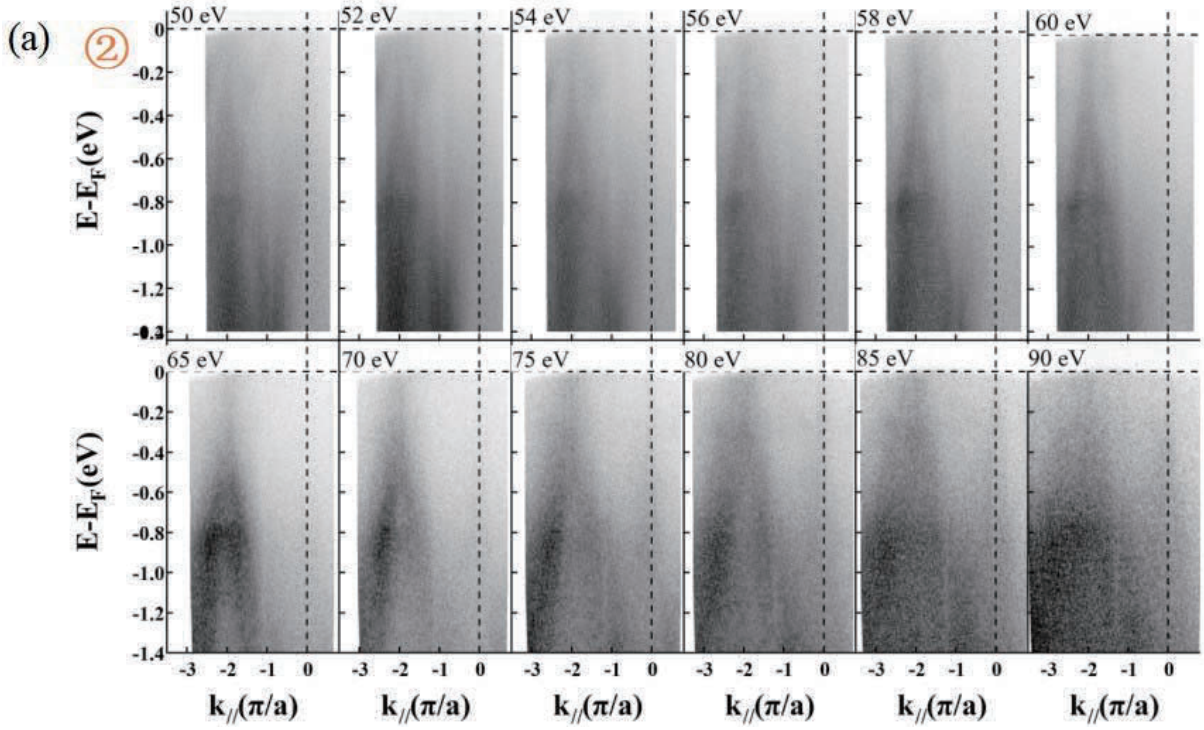

FIGURE 3. (a) The h*v*-dependent band structures along Γ-K direction measured with photo energy from 50 eV to 90 eV.

Fig. 1(b) displays the calculated bulk electronic structure of SrAgBi. By contrast, Fig. 2(b) incorporates surface state contributions, revealing finer band details where the computed surface bands align more closely with ARPES experimental data. In Fig. 1(b), linear Dirac-like band features emerge at E_B = −0.5 eV and −1 eV. These distinctly diverge from the bulk bands in Fig. 1(b) and are attributed to topological surface states according our DFT calculations as in Fig. 2(b). Fig. 1(a) depicts the momentum-space directions ("1" and "2") selected for ARPES measurements. Fig. 2 presents corresponding ARPES band results for both directions. Red arrows in Fig. 2(a) highlight flat bands—at E_B = −0.3 eV, −0.8 eV, and −3 eV—that is a discrepancy from DFT predictions. Their origin remains undetermined and necessitates additional ARPES beamtime for clarification. Basically, the DFT-calculated bulk electronic structure broadly matches experimental observations. First, three parabolic hole bands spanning E_B = −3 eV to the Fermi level are consistent with DFT results. Second, red arrows in Fig. 2(b) indicate pronounced band splitting at E_B = −0.8 eV and −3 eV. These bands correspond to direction "2" in Fig. 1(a) (i.e., the A–L–K momentum path). While the A–L segment exhibits a single flat band without splitting, splitting occurs along L–H momentum direction. Fig. 2(b) visualizes band dispersion across a broader

energy scale. Red arrows indicate band splitting, identifying as a hidden Dresselhuas spin-orbit coupling (SOC) hallmark, which is clearly resolved in the second-derivative spectrum. This directional bulk-band splitting and out-plane electron spin polarization signify the hidden Dresselhaus effect—a phenomenon requiring specific crystal and atomic-site symmetries and representing a frontier topic in spintronics [2]. Thus, these results provide the first direct evidence of this effect. Fig. 3 summarizes photon-energy-dependent ARPES experiments. After evaluating spectra across energies, hν = 60 eV was selected as optimal for subsequent ARPES measurements. Despite low cleavage success rates, partial ARPES data captured a double-hole-type Fermi pocket near the Γ–K line, exhibiting good agreement with theory. In Fig. 3, we can see the binding energies of flat bands did not move with the changing of photo energy, indicating they result from the possible surface reconstructions. While the bands near the E_F show the evident different with the changing of photo energy, indicating their bulk states feature. In the near future, high-resolution ARPES measurements will be conducted to improve the data presented in Fig. 3. Then one can directly observe the type Ⅳ Dirac band structures in SrAgBi.

So fat, our experimental study in BL-1 pioneers the observation of hidden Dresselhaus-type SOC band splitting and detailed band structures near Γ point. Future work demands further ARPES and spin-resolved ARPES experiments to:

(1) Determine flat-band origins: Since 4f-electron-related bands are absent, these flat bands require analysis via additional high-resolution ARPES data.

(2) Confirm unconventional spin polarization: Clear Dresselhaus splitting lacks spin-ARPES validation so far. Theoretical calculations predict out-of-plane spin polarization with kz-dependence and non-helical texture—distinct from Rashba effects and critical for spintronics physics.

Reference:

[1] Ma T C, Hu J N, Chen Y, et al. Coexistence of type-ii and type-iv dirac fermions in SrAgBi. Mod. Phys. Lett. B 35, 2150181 (2021).

[2] Zhang X, Liu Q, Luo J W, et al. Hidden spin polarization in inversion-symmetric bulk crystals. Nat. Phys. 10, 387-393 (2014).

Comprehensive Study of Electronic States Induced by Quantum Charge Fluctuations in Electron-doped High-T_c Cuprate Superconductors

H. Yamaguchi[a], Y. Onishi[a], Y. Miyai[a], M. Atira[b], H. Sato[a,b], D. Song[f], K. Tanaka[e], K. Shimada[a,b,c,d], S. Ideta[a,b]

[a]*Graduate School of Advanced Science and Engineering, Hiroshima Univ., Higashi-Hiroshima 739-0046, Japan*
[b]*Hiroshima Synchrotron Radiation Center (HiSOR), Hiroshima Univ., Higashi-Hiroshima 739-0046, Japan*
[c]*Research Institute for Semiconductor Engineering, (RISE), Hiroshima Univ., Higashi-Hiroshima 739-8527, Japan*
[d]*International Institute for Sustainability with Knotted Chiral Meta Matter (WPI-SKCM^2), Higashi-Hiroshima 739-8526, Japan*
[e]*UVSOR-III Synchrotron, Institute for Molecular Science., Okazaki, Aichi 444-8585, Japan fStewart*
[f]*Blusson Quantum Matter Institute,University of British Columbia,Vancouver, BCV 6T1Z4,Canada*

Keywords: cuprate superconductors, charge fluctuation, electronic structure, ARPES, IPES

The mechanism for high-T_c cuprate superconductivity is realized by interaction between electrons and bosons. However, it has been a long-standing mystery to what extent which bosons play an important role to occur high-T_c superconductivity.

Recent resonant inelastic x-ray scattering (RIXS) experiments have been reported that charge excitations for high-T_c cuprate superconductors [1-3]. The contribution of the charge fluctuations to high-T_c cuprate superconductivity has started to pay attention for the physics of cuprate superconductivity. According to previous theoretical studies [4-7], using the layered *t-J* model, the electron self-energy is calculated and discussed about the effect of charge fluctuation for the electronic structure of cuprates.

In this study, we have performed an angle-resolved photoemission spectroscopy (ARPES) and inverse photoemission spectroscopy (IPES) to understand the electronic structure for the electron-doped cuprate $Nd_{1.85}Ce_{0.15}CuO_4$ in the occupied and unoccupied states, respectively. In addition to the experiments, we have performed *ab-initio* calculations to investigate the electronic structure as shown in Fig. 1. We have observed band dispersions and found some similar features corresponding to charge derived bands. In the poster presentation, we will show the experimental and theoretical results in details and discuss the effect from the charge fluctuation of cuprate superconductors.

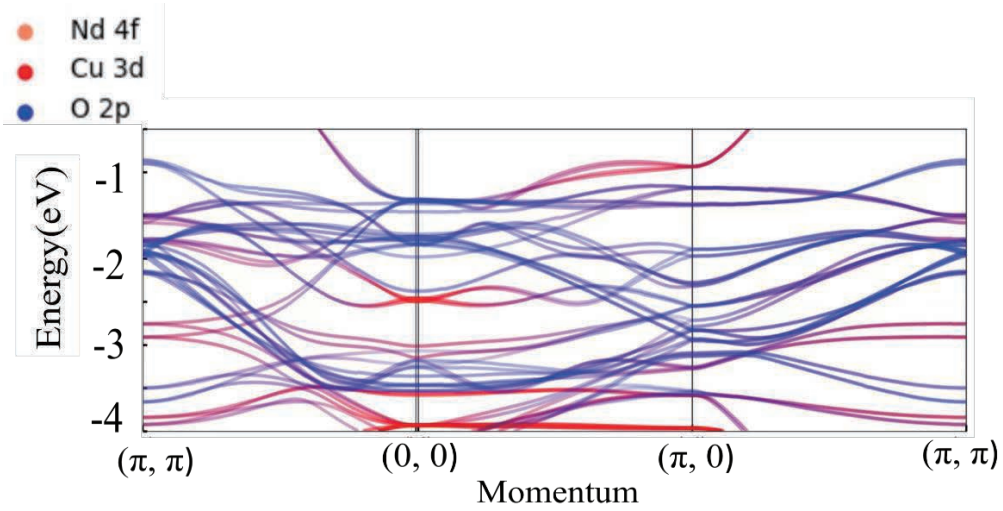

FIGURE 1. Bulk-band structure of Nd_2CuO_4 using DFT calculations. The color and intensity of the curves correspond to the weight of orbitals, Nd 4*f*, Cu 3*d*, and O 2*p*.

REFERENCES

1. J. Lin *et al*., Quantum Materials **5**, 4 (2020).
2. A. Singh *et al*., Phys. Rev. B **105**, 235105 (2022).
3. W. S. Lee *et al*., Nature Phys **10**, 883-889 (2014).
4. A. Greco *et al*., Commun Phys **2**, 3 (2019).
5. H. Yamase *et al*., Phys. Rev. B. **104**, 045141 (2021).
6. H. Yamase *et al*., Phys. Rev. B **109**, 1 (2024).
7. H. Yamase *et al*., Commun Phys **6**, 168 (2023).

ARPES study of Fe_xTiS_2 ($x = 0 \leq x \leq 0.33$)

Y. Nakashima[a], K. Kimura[a], Y. Tanimoto[a], H. Sato[b], M. Arita[b], Y. Miyai[a], S. Ideta[b], K. Shimada[b], T. Bizen[c], M. Miyata[c], M. Koyano[c]

[a]*Graduate School of Advanced Science and Engineering, Hiroshima University, Higashi-Hiroshima 739-8526, Japan*
[b]*Research Institute for Synchrotron Radiation Science, Hiroshima University, Higashi-Hiroshima 739-0046, Japan*
[c]*School of Materials Science, Japan Advanced Institute of Science and Technology, Nomi 923-1292, Japan*

Keywords: intercalation, superlattice, angle-resolved photoemission spectroscopy

1*T*-TiS_2 is a non-magnetic layered material with a 1*T*-CdI_2-type crystal structure. Each hexagonal layer of Ti ions is sandwiched between two hexagonal layers of S ions, and each Ti ion is octahedrally coordinated by six S ions. Within a layer, the S-Ti-S trilayers are covalently bonded, while adjacent TiS_2 trilayers are weakly coupled through van der Waals (vdW) forces. The vdW gap between the TiS_2 layers can host intercalated 3*d* transition-metal ions, forming compounds of the type M_xTiS_2. Among these, Fe_xTiS_2 exhibits a rich variety of magnetic properties [1].

As the Fe concentration increases from $x = 0$, a cluster spin-glass (CG) state with Ising spins is observed for $x < 0.20$. An antiferromagnetic (AFM) state emerges for $0.20 \leq x \leq 0.28$, followed by another CG state for $0.28 < x < 0.38$, and then an AFM state again for $0.38 < x < 0.50$. For $x > 0.50$, ferrimagnetic behavior appears. The intercalated Fe ions occupy octahedral sites within the vdW gap, surrounded by six S ions. X-ray studies reveal that Fe ions are randomly distributed for $x < 0.20$, while ordered superlattices form at higher concentrations: a $2\sqrt{3}a \times 2a \times 2c$ superlattice at x = 0.25 and a $\sqrt{3}a \times \sqrt{3}a \times 2c$ superlattice at $x = 0.33$. The diversity of magnetic phases in Fe_xTiS_2 is expected to originate from modifications of the electronic band structure induced by Fe intercalation.

In this study, we performed angle-resolved photoemission spectroscopy (ARPES) on Fe_xTiS_2 ($0 \leq x \leq 0.33$) at beamlines BL-1, BL-7 and BL-9A of the Research Institute for Synchrotron Radiation Science (HiSOR). We also investigated the unoccupied electronic band structure of TiS_2 using angle-resolved inverse photoemission spectroscopy (ARIPES) with a resonance IPES spectrometer at HiSOR [2].

Figures 1(a) and 1(b) present ARPES intensity plots of TiS_2 and $Fe_{0.33}TiS_2$, respectively, measured at $h\nu$ = 66 eV along the $\bar{\Gamma}$-$\bar{M}$ direction of the surface Brillouin zone, which approximately corresponds to the bulk Γ-M direction as estimated from $h\nu$-dependent measurements. The spectra were recorded at 20 K with *p*-polarized geometry. In TiS_2 (Fig. 1(a)), an electron pocket derived from Ti 3*d* states is observed around the M point, with its intensity resonantly enhanced near the Ti 3*p*-3*d* absorption region. A nearly non-dispersive band appears just below the pocket, attributed to localized 3*d* states of self-intercalated Ti ions in the vdW gap. The electron pocket is barely visible with *s*-polarized geometry (not shown), indicating that it mainly arises from the Ti $3d_{z^2}$ orbital. A parabolic band at the Γ point originates from S 3*p* states.

For $Fe_{0.33}TiS_2$ (Fig. 1(b)), the electron pocket around the M point shifts to higher binding energy compared with TiS_2, leading to its enlargement. The parabolic S 3*p* band also shifts to deeper energy. These features indicate electron transfer from intercalated Fe ions to the TiS_2 host layers. A dispersive Fe 3*d*-derived band appears around $E_B = 0.4$ eV, as indicated by dashed lines in Fig. 1(b), reflecting the periodic alignment of Fe ions in the vdW gap.

Figure 2 shows ARIPES intensity plots of TiS_2 along the $\bar{\Gamma}$-$\bar{M}$ direction at 300 K. The spectra were obtained by scanning the emitted photon energy while keeping the incident electron kinetic energy fixed at $E_k = 50$ eV and varying the incidence angle in $\Delta\theta = 2$ deg. steps relative to the surface normal. The vertical axis represents the energy above the Fermi level. A dispersive band appears around $E = 2$ eV, which is resonantly enhanced near $E = 46$ eV and therefore attributed to unoccupied Ti 3*d* bands [3]. Another band is observed around $E = 4$ eV. However, no unoccupied counterpart of the ARPES electron pocket is detected.

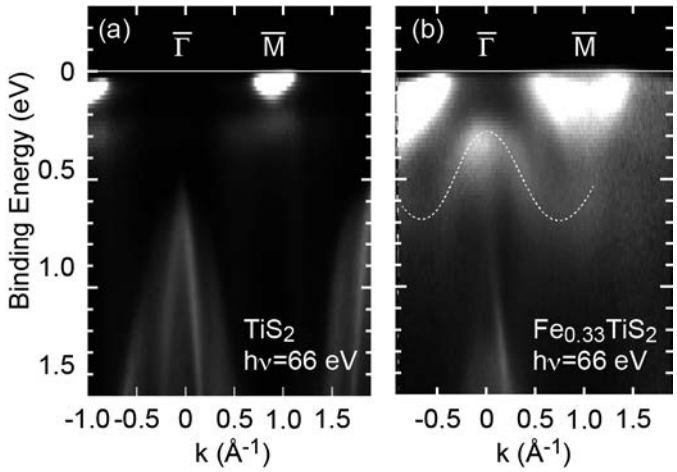

FIGURE 1. ARPES images of (a) TiS_2 and (b) $Fe_{0.33}TiS_2$ measured at $h\nu = 66$ eV along $\bar{\Gamma}$-$\bar{M}$ direction. Dashed lines in (b) is guide for the eye for the Fe 3*d* band.

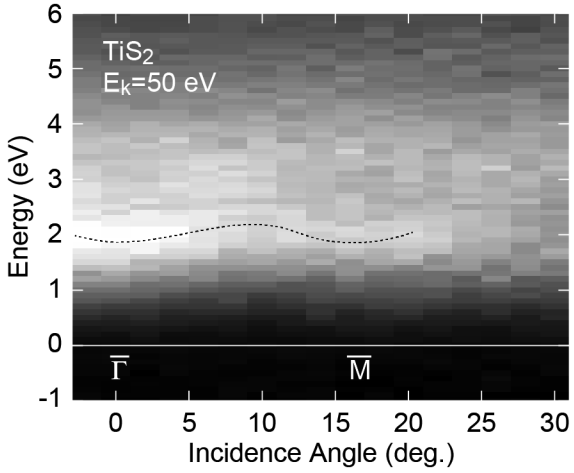

FIGURE 2. ARIPES image of TiS_2 measured at E_k = 50 eV along $\bar{\Gamma}$-$\bar{M}$ direction. Dashed line is guide for the eye for the unoccuoied Ti 3*d* band.

REFERENCES

1. N. V. Selezneva, E. M. Sherokalova, A. Podlesnyak, M. Frontzek and N. V. Baranov, Phys. Rev. Mater. **7**, 014401 (2023).
2. H. Sato, T. Kotsugi, S. Senba, H. Namatame and M. Taniguchi, J. Synchrotron Radiat. **5**, 772 (1998).
3. M. Arita, H. Sato, M. Higashi, K. Yoshikawa, K. Shimada, M. Nakatake, Y. Ueda, H. Namatame, M. Taniguchi, M. Tsubota, F. Iga and T. Takabatake, Phys. Rev. B **75**, 205124 (2007).

Probing Correlated Electron Behavior in MnTe Using ARPES and IPES

Kazi Golam Martuza[a], Yogendra Kumar[b], Hiroshi Yamaguchi[a] Shiv Kumar[c], Mashashi Arita[b], Hitoshi Sato[b], Shin-ichiro Ideta[b] and Kenya Shimada[b,d,e]

[a]Graduate School of Advanced Science and Engineering, Hiroshima University, Japan 739-8526
[b]Research Institute for Synchrotron Radiation Science (HiSOR), Hiroshima University, Japan 739-0046
*[c]Institute of Microelectronics, Agency for Science, Technology and Research (A*STAR), Singapore*
[d]International Institute for Sustainability with Knotted Chiral Meta Matter (WPI-SKCM^2), Hiroshima University, Higashi-Hiroshima 739-8526, Japan
[e]Research Institute for Semiconductor Engineering (RISE), Hiroshima University, Higashi-Hiroshima 739-8527, Japan

Keywords: MnTe, Altermagnetism, ARPES, IPES, Electron Correlation, Photoemission Spectroscopy.

Altermagnetism is a newly identified magnetism with zero net magnetization in which magnetic sublattices are interrelated by crystal rotation symmetries, rather than by translation or inversion [1–3]. We investigated the occupied electronic states of MnTe(0001) single crystals, a representative altermagnet, using angle-resolved photoemission spectroscopy (ARPES), resonant photoemission spectroscopy and resonant inverse photoemission spectroscopy. A reproducible surface preparation method, involving argon ion sputtering followed by thermal annealing, was established to obtain a clean and well-ordered surface, confirmed by Auger electron spectroscopy (AES) and low-energy electron diffraction (LEED).

The MnTe(0001) surface was prepared through repeated cycles of sputtering at 2 kV and annealing at 673 K for 60 minutes. AES confirmed a near 1:1 Mn:Te atomic ratio, and sharp LEED spots exhibited six-fold symmetry, indicating long-range order.

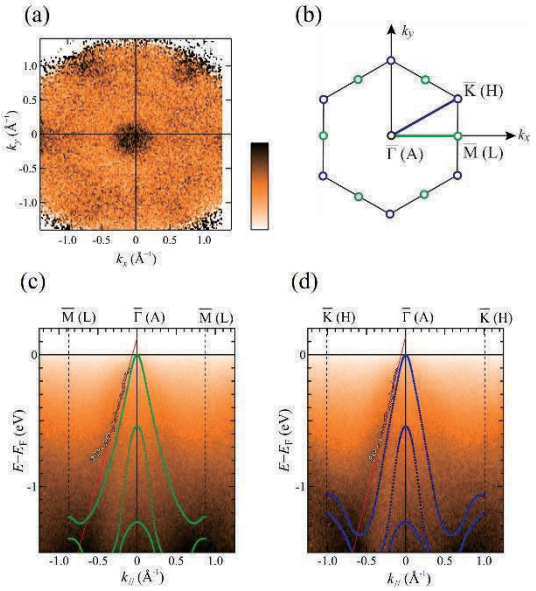

FIGURE 1. ARPES results for a MnTe(0001) single crystal measured at 20 K using photon energy $h\nu$ = 117 eV in the *p*-polarization geometry. (**a**) k_x–k_y map near the Fermi level, obtained by integrating spectral intensity over the energy range from −0.1 eV to 0 eV. The k_x direction corresponds to the $\bar{\Gamma}\bar{M}$ direction. (**b**) Surface (bulk) Brillouin zone. ARPES intensity plots along (**c**) $\bar{\Gamma}\bar{M}$ and (**d**) $\bar{\Gamma}\bar{K}$ directions. Open circles indicate peak positions obtained by MDC fitting. Red lines represent fits to obtained data points from −0.6 to −0.1 eV. DFT + *U* calculations along the AL (green circles in (**c**)) and AH (blue circles in (**d**)) directions are overlaid.

ARPES measurements were performed at hν = 117 eV using p-polarized light, with an energy resolution of 20–50 meV. Data were collected at 20 K under a base pressure of 3.6×10^{-9} Pa. Figure 1 summarizes the ARPES results for MnTe(0001) taken at BL-1. In Fig. 1(a), a constant-energy map obtained by integrating spectral intensity from −0.1 eV to the Fermi level reveals a six-fold symmetric intensity distribution, consistent with the hexagonal surface symmetry. Figs. 1(c) and 1(d) show ARPES results along ΓM and ΓK, respectively, compared with the DFT + U calculations (green and blue circles). Our ARPES results are consistent with previously reported ARPES results on bulk single crystals of cleaved surface [4].

To examine the experimental band points in more detail, we fitted the momentum distribution curves (MDCs: ARPES intensity as a function of wavenumber at a given energy) using a single Lorentzian for $k_{//} < 0$ Å^{-1} and from −0.8 eV up to −0.1 eV. The experimental band points are represented by open circles in Figs. 1(c) and 1(d). Subsequently, we fitted the experimental band points within the energy range from −0.6 eV up to −0.1eV using a linear function, as indicated by the red lines in the figures. Then, the Fermi wave number was estimated as $k_F \approx \pm 0.1$ Å^{-1}. To achieve agreement with this experimental k_F value, the theoretical band dispersion should be shifted toward higher energies (hole doping direction) by approximately 0.1 eV.

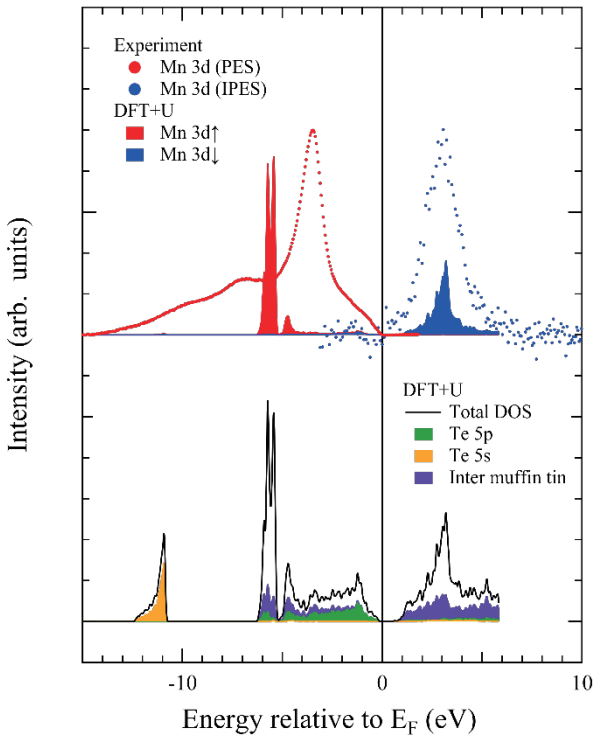

FIGURE 2. The theoretical partial density of states (DOS) inside the Muffin tin potential given by our DFT+U calculations: Mn 3d↑ partial DOS (red area), Mn 3d↓ partial DOS (blue area), total DOS (black line), Te 5p partial DOS (green area), Te 5s partial DOS (yellow area), and the DOS in inter muffin-tin region (violet area). Experimentally determined occupied Mn 3d state (red circles) and the unoccupied Mn 3d state (blue circles) are also shown.

The upper panel of Fig. 2 shows the Mn 3d-derived spectra obtained via resonant photoemission and inverse-photoemission spectroscopies after background subtraction using the Shirley's method [5]. The observed energy positions of Mn3d↑ is -3.5 eV in the photoemission spectra and Mn 3d↓ is located at +3.0 eV in the inverse-photoemission spectra. The experimental U_{eff} value is 6.5 eV, which is consistent with previous results [6,7,8].

In Fig. 2, we also show the theoretical partial density of states (DOS) inside the muffin-tin potential given by our DFT+U calculations. The Mn 3d-$t_{2g\uparrow}$ derived DOS in the occupied state exhibits narrow peak at around -5.5 eV and the Mn 3d-$t_{2g\downarrow}$ derived DOS in the unoccupied state has a peak at +3.5 eV. The Te 5p states extend from -6 eV up to the top of the valence band maximum. The contribution from Te 5p partial DOS is

dominant from -4 eV up to the Fermi level. Note that there are broad states in the inter Muffin tin region forming almost flat DOS from -6 eV up to +6 eV. As the Te 5p states are primarily located in the occupied states, the unoccupied Mn 3d↓ states are energetically separated from the Te 5p states by the band gap.

The experimentally observed Mn 3d↑ energy position significantly deviates from the DFT+U calculation, whereas the observed Mn 3d↓ energy position agrees well. The theoretical peak separation of Mn 3d↑ and Mn 3d↓ amounts up to 9 eV, which is about 2.5 eV larger than the experimental value. If we set U = 0 eV in the calculation, the peak separation is reduced to 4 eV; however, the band gap also disappears. Although theoretical Mn 3d peak positions could be adjusted by U values, the ground-state property, such as magnetic moment, is well reproduced by $U_{eff} \sim 4 - 5$ eV [9]. In addition, it is impossible to reproduce satellite structure in the gap region between -10 eV and -7 eV within the DFT+U scheme.

By establishing a reproducible methodology for surface preparation, we have conducted ARPES and IPES measurements on MnTe(0001) single crystals. While the observed band dispersions near the Fermi level are well reproduced by the DFT+U calculations, we have found that the experimental energy position of the Mn 3d↑ peak significantly deviates from DFT + U, indicating the influence of many-body interactions. These findings provide a valuable reference for understanding electronic structure of altermagnetic materials.

REFERENCES

1. Šmejkal, L.; Sinova, J.; Jungwirth, T. *Phys. Rev. X* **2022**, *12*, 031042.
2. Mazin, I.; PRX editors. Editorial, *Phys. Rev. X* **2022**, *12*, 040002.
3. Din, A.D.; Amin, O.J.; Wadley, P.; Edmonds, K.W, *npj Spintron.* **2024**, *2*, 25.
4. Osumi, T.; Souma, S.; Aoyama, T.; Yamauchi, K.; Honma, A.; Nakayama, K.; Takahashi, T.; Ohgushi, K.; Sato, T., *Phys. Rev. B* **2024**, *109*, 115102.
5. Yeh, J.J.; Lindau, I., *At Data Nucl Data Tables* **1985**, *32*, 1, 1–155.
6. Sato, H.; Tamura, M.; Happo, N.; Mihara, T.; Taniguchi, M.; Mizokawa, T.; Fujimori, A.; Ueda, Y., *Solid State Commun* **1994**, *92*, 11, 921–924.
7. Sato, H.; Tamura, M.; Happo, N.; Mihara, T.; Taniguchi, M.; Mizokawa, T.; Fujimori, A.; Ueda, Y., *J Magn Magn Mater* **1995**, *140*, 153–154.
8. Sato, H.; Mihara, T.; Furuta, A.; Tamura, M.; Mimura, K.; Happo, N.; Taniguchi, M.; Ueda, Y., *Phys Rev B* **1997**, *56*, 12, 7222–7231.
9. Youn, S.J.; Min, B.I.; Freeman, A.J., *Physica Status Solidi (b)* **2004**, *241*, 7, 1411–1414.

Comparative ARPES Study Of Transition Metal Doped Topological Compounds $M_{0.05}Bi_{1.95}Se_3$ (M=Au, Pt, and Pd)

Shailja Sharma[a], Shiv Kumar[b] and C S Yadav[a]

[a] *School of Physical Sciences, Indian Institute of Technology Mandi, Kamnd, Mandi-175005 H.P. India*

[b] *Hiroshima Synchrotron Radiation Center, Hiroshima University, Hiroshima Japan,*

Keywords: Topological insulator, ARPES, Transport study

Topological insulators (TIs) are a class of quantum materials with the insulating bulk and metallic surface states which are protected by time reversal symmetry. The experimental discovery of 3D TIs in Bi_2Se_3, Bi_2Te_3 and Sb_2Te_3 have initiated a tremendous interest among the condensed matter research community, over the past decade. Among these, Bi_2Se_3 have been the most studied TIs because of the simple band structure with a single Dirac cone.[1] The band structure studied experimentally using the angle-resolved photoemission spectroscopy (ARPES) can provide the experimental value of the electronic band gap confirming the theoretically predicted values. The Fermi level in undoped Bi_2Se_3 lies usually inside the conduction band, thus confirming the n-type nature.[2]

We are interested in studying the doped Bi_2Se_3 with noble metals such as Au, Pt, and Pd which are transition heavy elements, thus would enhance the spin-orbit coupling in the parent compound. As discussed by Yan *et al*. that Au, Ag, Pt, Pd, Cu confirms to be the topological metals wherein topological surface states exist on the surface using ARPES results. [3] We are interested to see whether the Fermi level of the material is pushed into the bulk band gap or it is in the conduction band with the doping. It is crucial to see that the surface state originating from the topological insulator nature of Bi_2Se_3 still exists even after the noble metals doping. These changes in the surface states can be observed using ARPES measurements. The ARPES studies together with (Shubnikov-de-Hass) SdH effect would be a novelty to study the Fermi surface on such interesting systems.

Bi_2Se_3 is a well-known topological insulator, important from different aspects such as topological superconductivity and magnetism. We have grown high quality single crystals of the Au, Pt and Pd intercalated Bi_2Se_3, using melt-grown method which promises to exhibit expected ARPES results. We have already studied low temperature magneto-transport properties on these single crystals using PPMS by Quantum design. ARPES, Shubnikov-de-Haas (SdH) and de-Haas-van Alphen experiments promises importance towards studying the topological surface states.

We planedn to do a comparative study of the Bi_2Se_3 doped with 2.5% Au, Pt and Pd, which are heavy transition metal elements. The elements are expected to bring change in the electronic structure of Bi_2Se_3 due to higher spin-orbit coupling, besides inducing the charge carriers into the system. To the best of our knowledge, the detailed study of the Bi_2Se_3 doped/intercalated by the mentioned heavy transition metal elements has not been reported in literature. The proposed ARPES studies together with the magneto-transport studies and (Shubnikov-de-Hass) SdH effect would help in understand the physics of these topological materials.

Single crystals of the compounds were sent to the center for the measurements and the instrument scientist tried to do the measurements. However a good quality data could not be obtained in spite of efforts. Later the instruments scientist who was involved with the project moved from the center and The PhD students involved in this project also completed her PhD and moved to Germany for further postdoc work, so the study could not be completed.

REFERENCES

1. K. Kuroda *et al. Hexagonally Deformed Fermi Surface of the 3D Topological Insulator Bi_2Se_3*, Phys. Rev. Lett. **105**, 076802 (2010).
2. James G. Analytis *et al*. *Bulk Fermi surface coexistence with Dirac surface state in Bi_2Se_3: A comparison of photoemission and Shubnikov–de Haas measurements*, Phys. Rev. B **81**, 205407 (2010).
3. Binghai Yan *et al*. *Topological states on the gold surface*, Nat. Comm. **6**, 10167 (2015).

Photoelectron spectroscopy and local structure of the Se chain confined in single carbon nanotube

R. Nishikawa[a], K. Mimura[b], Y. Tanimoto[c], H. Sato[d], S. Islam[a], T. Miyanaga[e], and H. Ikemoto[a]

[a]*Department of Physics, University of Toyama, Toyama 930-8555, Japan*
[b]*Department of Physics and Electronics, Osaka Metropolitan University, Sakai 599-8531, Japan*
[c]*Graduate School of Advanced Science and Engineering, Hiroshima University, Higashi-Hiroshima 739-8526, Japan*
[d]*Hiroshima Research Institute for Synchrotron Radiation Science, Hiroshima University, Higashi-Hiroshima 739-0046, Japan*
[e]*Department of Mathematics and Physics, Hirosaki University, Hirosaki 036-8561, Japan*

Keywords: Se chain, carbon nanotube, Photoelectron spectroscopy, EXAFS.

Trigonal selenium (t-Se) is the stable crystalline form in which Se atoms form three-turn helical chains with twofold covalent bonds, and these chains are stacked through interchain interactions. This hierarchical structure—where the helical chains constitute the primary structure and the stacked chains constitute the secondary one—is a characteristic feature of chalcogen elements, including Se. This unique characteristic arises from the four 4p valence electrons: two form covalent bonds, while the others form lone-pair (LP) bonds. The LP bonds are located at the top of the valence band, with a gap between the LP bands and the anti-bonding (σ*) bands, making t-Se a semiconductor. The physical properties are strongly correlated with its structure. Therefore, it is crucial to study both the electronic state and local structure. In this report, we present the electronic structure and the local structure of selenium chains confined within single-walled carbon nanotubes (Se@SWCNT), as determined by extended X-ray absorption fine structure (EXAFS) and photoelectron spectroscopy (PES) measurements.

Se@SWCNT was synthesized by heat treatment of a glass tube sealing Se and SWCNT. PES experiments were perfomed at BL-7 in HiSOR using 120 eV excitation photon energy at both room temperature (RT) and 20 K (LT). EXAFS measurements for the Se K-edge (12.7 keV) were conducted at BL12C in KEK-PF using transmission mode over a temperature range of 20–300 K.

Figure 1 shows the PES spectra of SWCNTs with and without Se, where the backgrounds were subtracted using the Shirley method [1]. Since the Se atoms are confined within the SWCNTs, their contribution is relatively small. The PES spectra of Se@SWCNT were obtained by subtracting the spectra of SWCNTs without Se from those with Se. A key observation is the spectral weight near the Fermi energy (E_F); nearly zero at RT while finite at LT. This suggests that Se@SWCNT could exhibit metallic behavior at LT, while at RT it behaves like a semiconductor similar to t-Se.

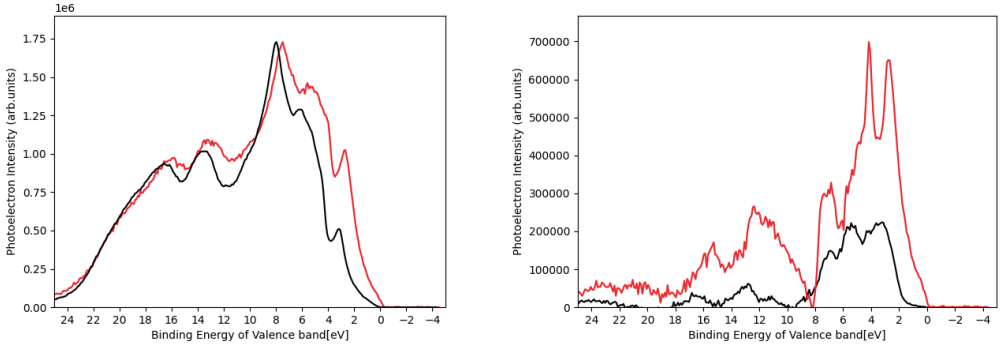

FIGURE 1. (a) The PES spectra of SWCNTs with and without Se at LT, (b)The PES spectra of Se@SWCNT at RT and LT.

The most interesting result from the EXAFS analysis is the temperature-dependent variation of the coordination number (N) of Se covalent bonds. At RT, the value of N is close to two, indicating that the two-fold covalent bonds remain intact even in Se@SWCNT. However, the value decreases to about 1.8 at LT. If we simply consider it, this suggests that the covalent bonds partially break as the temperature decreases.

We will discuss these interesting results in conjunction with the PES and EXAFS studies with other consideration.

REFERENCES

1. A. Shirley, Phys. Rev. B 5, 4709-4714 (1972).

Preparation of Pt Thin Film on MgO (001) and Observation of Its Electronic Structure

T. Asano[a], K. Sumida[b], K. Kunitomo[a], T. Okuda[b], and K. Miyamoto[b]

[a]*Graduate School of Advanced Science and Engineering, Hiroshima University, 1-3-1 Kagamiyama, Higashi-Hiroshima 739-8526, Japan*
[b]*Hiroshima Synchrotron radiation Center (HSRC), Hiroshima University 2-313 Kagamiyama, Higashi-Hiroshima 739-0046, Japan*

Keywords: Pt thin film, Spin Hall effect, Photoemission spectroscopy

Spin Hall effect is an important physical phenomenon that generates spin-polarized currents and is essential for the development of spintronics devices. The spin Hall effect in metals has attracted attention because conductance mismatches are markedly suppressed at an interface with ferromagnet compared to the semiconductors and allows the use of spin-polarized current supplied by the ferromagnetic metal [1]. Among many metals, elemental Pt is extensively investigated both experimentally and theoretically [2,3]. Kimura *et al.* reported that the Pt wire exhibits largest spin Hall conductivity as large as 2.4×10^4 S/m at room temperature, which is 4 orders of magnitude larger than that of typical semiconductors, such as GaAs [2]. In order to inject spin-polarized current into ferromagnets more efficiently, the orientation of spin current must be precisely controlled, i.e., it is necessary to observe its spin orientation. In previous studies, the rough spin orientation of spin currents induced by spin Hall effects has been obtained by using the magneto-optical Kerr effect [4]. However, the experimental method to precisely detect the spin orientation induced by the spin Hall effect has not been established yet. One solution is *operando* spin-resolved photoemission spectroscopy (PES) measurements under an external electric field.

In this work, as a first step towards the development of the experimental method, we fabricated Pt thin films and investigated the electronic structure by PES measurements. The Pt thin films were prepared by using electron beam evaporation source with a carbon crucible on a MgO(001) substrate at room temperature. The MgO substrate was annealed in oxygen atmosphere (~10^{-1} Pa) at ~200°C for 60 min., and then, annealed at 600°C for 240 min. in vacuum prior to the Pt deposition.

To observe the electronic structure of the fabricated Pt/MgO film, we performed the PES measurements at BL-7 of Hiroshima Synchrotron Radiation Center utilizing various incident photon energies from 30 to 160 eV. Figure 1 shows Pt 4*f* core level spectrum taken at $h\nu$ = 155 eV. Two peaks derived from the spin-orbit split Pt $4f_{5/2}$ and $4f_{7/2}$ are clearly seen at binding energy (E_B) of 74.4 and 71.1 eV. To obtain more detailed information, the experimental result was fitted by Doniac-Šunjić function with Shirley background function [see blue curve in Fig. 1]. From this fitting result, asymmetric parameters were determined to be 0.018 for $4f_{5/2}$ and 0.043 for $4f_{7/2}$. These values are very small as a metal, suggesting that the density of states (DOS) near the Femi level (E_F) is small.

The red curve in Fig. 2 shows the experimentally observed valence band PES spectrum taken at $h\nu$ = 70 eV. We can see broad peak structures around E_B = 1.6 and 4.5 eV. Moreover, a dip structure is recognized at E_B = 3.2 eV. To compare the valence band spectrum, we carried out the first-principles calculation for the face-centered-cubic Pt using WIEN2k program including the spin-orbit coupling. Based on the calculation, it was found that the *d* orbital component is dominant in the valence band rather than the *s* and *p* orbitals. Moreover, photo-onization cross-section of *d* orbital is dominated in the vacuum ultraviolet region. Therefore, in Fig. 2, we compare the PES spectrum with the Pt *d* partial DOS. Here, the calculated Pt *d* partial DOS was multiplied by the Fermi-Dirac distribution function at 300 K and convoluted by a Gaussian function (experimental resolution). Comparing the experimental and theoretical results, we notice that the locations of the peak and dip structures and the band width are qualitatively reproduced. However, a very

sharp peak predicted by the calculation in the vicinity of E_F was not observed in the experiment. This suggests that the interface and/or surface structure of the fabricated Pt film on MgO substrate makes the electronic structure differ from the electronic structure in the bulk Pt.

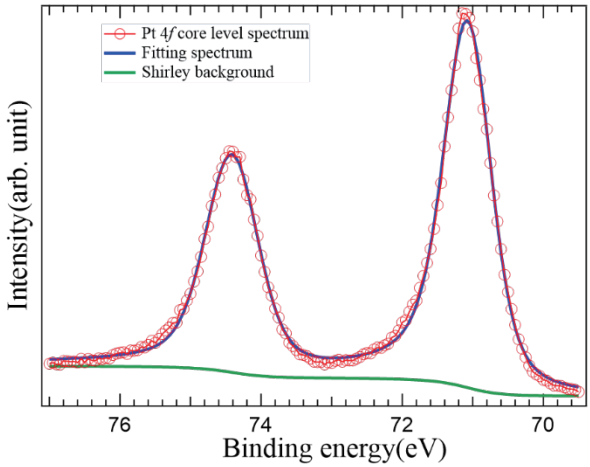

FIGURE 1. Pt 4*f* core level spectrum (red circles) taken at $h\nu = 155$ eV. The blue curve represents the fitting result using the Doniach-Šunjić function and active Shirley background (green curve).

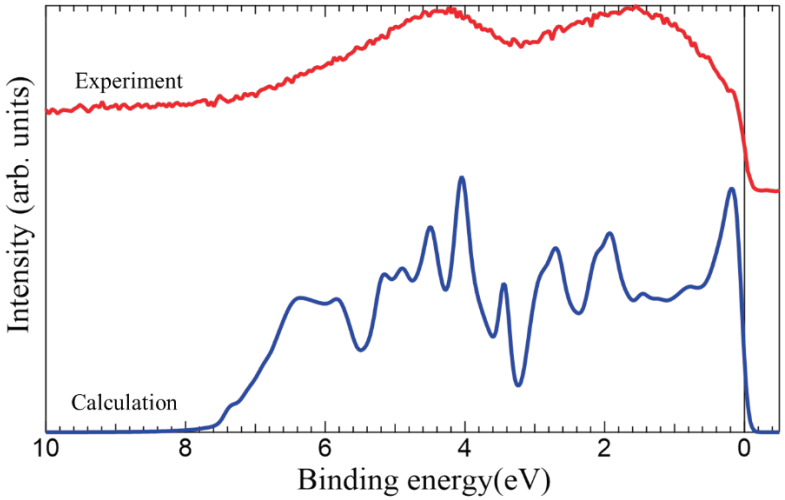

FIGURE 2. Observed photoemission spectrum taken at $h\nu = 70$ eV (red) and the calculated Pt *d* partial DOS (blue). The calculated DOS is multiplied by the Fermi-Dirac distribution function and convoluted by a Gaussian function.

In conclusion, we are successful to prepare Pt thin film on MgO(001) using electron beam evaporate source with a carbon crucible. Around E_F, the observed electronic structure on Pt thin film is differrent from calculated spectrum based on the bulk Pt. In general, the performance of the spin Hall effect is closely related to the electronic structure, so this finding of discrepancy may be important information for improving the performance of the spin Hall effect for Pt thin film on MgO(001).

REFERENCES

1. G. Schmidt, *et al*, Phys. Rev. B **62**, R4790(R) (2000).
2. T. Kimura *et al*., Phys. Rev. Lett. **98**, 156601 (2007).
3. G. Y. Guo, *et al.*, Phys. Rev. Lett **100**, 096401(2008).
4. Y. K. Kato, *et al*, Science **306**, 5703 (2004).

Valence band photoemission spectra of novel quadruple perovskite oxide $CeCu_3Ru_{3.25}O_{12}$

Hiroaki Anzai[a], Yasuaki Kikuchi[a], Yuta Kato[a], Kyoichi Otsuki[a], Masahiro Yamada[a], Ryuki Ishibashi[a], Yukimi Tanimoto[b], Hitoshi Sato[c], Masashi Arita[c], and Ikuya Yamada[a]

[a] *Graduate School of Engineering, Osaka Metropolitan University, Sakai 599-8531, Japan*
[b] *Graduate School of Advanced Science and Engineering, Hiroshima University, Higashi-Hiroshima 739-8526, Japan*
[c] *Research Institute for Synchrotron Radiation Science, Hiroshima University, Higashi-Hiroshima 739-0046, Japan*

Keywords: Kondo effect, *A*-site-ordered perovskite oxide, photoemission spectroscopy.

The *A*-site substituted quadruple perovskite ruthenate $ACu_3Ru_4O_{12}$ provides a unique opportunity for studying a *d*-electron heavy-mass behavior. The coefficient of the electron specific heat for *A* = Ca is $\gamma \sim 84$ mJ/(mol·K^2), indicating a heavy effective mass [1]. Interestingly, γ systematically increases with the valence of the *A*-site cation, implying a correlation between *A*-site valence and the degree of electron localization or hybridization [2]. The correlation commonly manifests as a characteristic quasiparticle peak at the Kondo temperature in the electronic excitation spectra near the Fermi energy [3]. Therefore, investigating the temperature evolution of spectra provides critical for understanding the mechanisms governing heavy-fermion behavior. We have recently obtained a $CeCu_3Ru_xO_{12}$ compound with $\gamma > 100$ mJ/(mol·K^2) by a high-pressure synthesis method. The dual character of Ce $4f^0$ and $4f^1$ electronic states, balancing localization and hybridization, offers a valuable platform to investigate the role of *A*-site valence and its influence on electronic structure.

Here, we present a photoemission spectroscopy study on the novel quadruple perovskite oxides $CeCu_3Ru_xO_{12}$ (x = 4.0, 3.25). The experiments were performed at BL-7 of Research Institute for Synchrotron Radiation Science. The photoemission data were collected with the photon energy of $h\nu$ = 200 and 60 eV. The energy resolution was 68 meV at $h\nu$ = 60 eV. The samples were cleaved *in situ* and kept under an ultrahigh vacuum of 3.6×10^{-9} Pa.

Figure 1(a) shows the core-level photoemission spectra of $CeCu_3Ru_xO_{12}$ (x = 4.0 and 3.25) measured at T = 10 K, along with the reference spectrum of the *A* = Ca compound. The line shapes for the *A* = Ca and Ce samples are qualitatively similar, exhibiting core-level features corresponding to Cu 3*p*, Ru 4*s*, Ru 4*p*, O 2*s*, and O 2*p* states

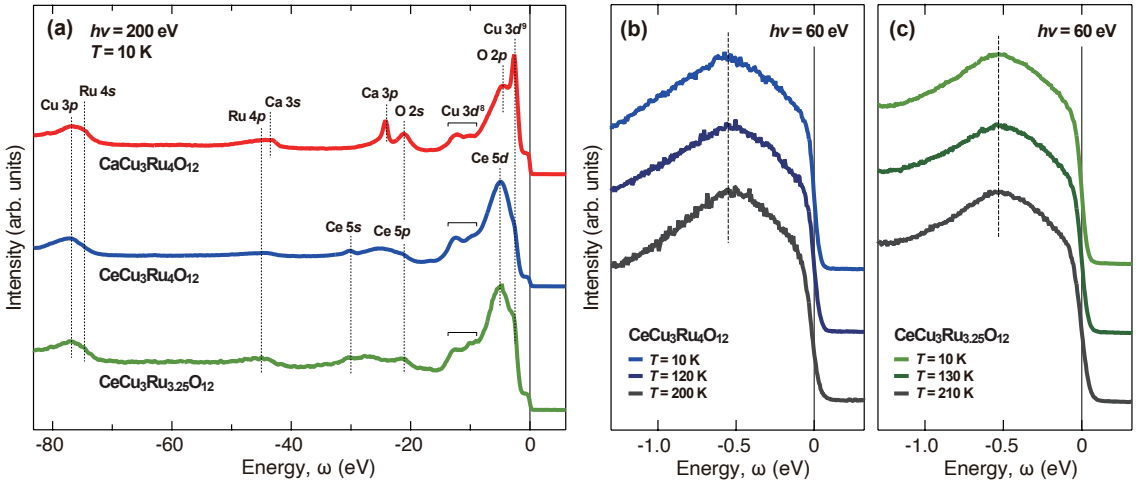

Figure 1. Overview of core and valence photoemission spectra of $CeCu_3Ru_xO_{12}$ (x = 3.25 and 4.0). (a) Photoemission spectra of the *A* = Ce and Ca samples over a wide energy range. The spectra were measured at T = 10 K with a photon energy of $h\nu$ = 200 eV. Vertical dashed lines indicate the energy positions of the core levels. The multiplet structure of $3d^8$ final states is marked by a horizontal line at |ω| - 16 eV. (b)(c) Temperature dependence of the photoemission spectra for x = 4.0 and 3.25, respectively, measured with $h\nu$ = 60 eV. Vertical dashed lines indicate characteristic energy scales in the valence spectra.

at binding energies consistent with standard reference data [4,5]. In addition, the presence of core levels specific to each *A*-site cation, such as the Ce 5*p* state at 21 eV and the Ca 3*p* state at 28 eV, confirms the reliability of the photoemission measurements. In the valence region, a multiple peak at $9 < |\omega| < 14$ eV and a sharp peak at 2.5 eV are assigned to the Cu $3d^8$ and $3d^9$ states, respectively [6,7]. The observation of a well-defined Fermi edge in both samples indicates their metallic electronic structure.

In Figs. 1(b) and 1(c), we show the photoemission spectra near E_F for $x = 4.0$ and 3.25, measured with photon energy of $h\nu = 60$ eV. At $T = 10$ K, a broad peak is observed at approximately 0.55 eV for $x = 4.0$ and 0.53 eV for $x = 3.25$. A similar peak has been reported for the A = Ca and Sr compounds and attributed to the Cu $3d_{xy}$ orbital states [6,7]. We found that the energy position and intensity of this peak exhibit negligible temperature dependence, as indicated by the dashed lines.

In the A = Ca compound, it has been reported that the resonance-like peak near E_F rapidly disappears above 100 K, which has been attributed to the loss of coherent hybridization between Cu 3*d* and Ru 4*d* electrons at elevated temperatures [8]. In the present measurements, the energy resolution is insufficient to resolve the fine feature of the quasiparticle peak near E_F. Therefore, higher-resolution photoemission experiments, such as those conducted at BL-9A, are necessary to elucidate the *d*-electron-based heavy-fermion behavior in $CeCu_3Ru_4O_{12}$.

REFERENCES

1. W. Kobayashi, I. Terasaki, J. Takeya, I. Tsukada, and Y. Ando, J. Phys. Soc. Jpn. **73**, 2373 (2004).
2. T. Tanaka, N. Shimazui, H. Takatsu, S. Yonezawa, and Y. Maeno, J. Phys. Soc. Jpn. **78**, 024706 (2009).
3. N. E. Bickers, D. L. Cox, and J. W. Wilkins, Phys. Rev. B **36**, 2036 (1987).
4. NIST X-ray Photoelectron Spectroscopy Database, NIST Standard Reference Database Number 20, Online, available at https://srdata.nist.gov/xps/, National Institute of Standards and Technology, Gaithersburg MD, 20899, 2000.
5. B. Vincent Crist. “Handbooks of Monochromatic XPS Spectra – The Elements and Native Oxides, Volume 1”. XPS Inter-national LLC: Mountain View, CA, USA, 1999.
6. H. Liu, Y. Cao, Y. Xu, D. J. Gawryluk, E. Pomjakushina, S.-Y. Gao, P. Dudin, M. Shi, L. Yan, Y.-F. Yang, and H. Ding, Phys. Rev. B **102**, 035111 (2020).
7. H. Anzai, Y. Kikuchi, Y. Kato, T. Iwazumi, Y. Tanimoto, H. Sato, M. Arita, and I. Yamada, J. Phys. Soc. Jpn. **94**, 084802 (2025).
8. T. Sudayama, Y. Wakisaka, K. Takubo, T. Mizokawa, W. Kobayashi, I. Terasaki, S. Tanaka, Y. Maeno, M. Arita, H. Namatame, and M. Taniguchi, Phys. Rev. B **80**, 075113 (2009).

Changes in Conduction-Band Density of States on Dy-TM Metallic Glasses Having Cryogenic Rejuvenation Effect II

Shinya Hosokawa,[a] Kentaro Kobayashi,[a] Koji Ohara,[a] Yukimi Tanimoto,[b] and Hitoshi Sato[c]

[a]*Faculty of Materials for Energy, Shimane University, Matsue 690-8504, Japan*
[b]*Graduate School of Advanced Science and Engineering, Hiroshima University, Higashihiroshima 739-8526, Japan*
[c]*Hiroshima Research Institute for Synchrotron Radiation Science, Hiroshima University, Higashihiroshima 739-0046, Japan*

Keywords: Temperature cycling, Rejuvenation, Metallic glasses, Partial density of states

Rejuvenation in glasses is generally defined as an excitation to a higher energy state by an external stress, opposite to the usual relaxation process by thermal annealing. A rejuvenation effect by temperature cycling in metallic glasses (MGs) was reported by Ketov et al. [1], which is caused by an internal stress with an external stimulation. According to their interpretation, if a glass is elastically heterogeneous, the thermal expansion coefficient has a distribution over the glass. Repeated temperature changes produce different magnitudes of thermal expansion in a glass, inducing shearing forces and resulting in a rejuvenation effect in the glass. The validity of this simple picture is the subject of intensive debate.

Hufnagel, who named this phenomenon 'cryogenic rejuvenation', reviewed the rejuvenation effect of thermal cycling and suggested that non-affine deformation must be induced on an atomistic length scale [2]. The extent of the heterogeneity in glasses can be determined from the so-called β-relaxation peak in dynamic mechanical analysis (DMA) spectra [3]. Yamazaki measured DMA spectra on $Gd_{100-x}Co_x$ glasses [4], and a distinct β-relaxation peak was observed in the $Gd_{65}Co_{35}$ glass, where the largest heterogeneity was expected.

We have carried out high energy X-ray diffraction (HEXRD) and anomalous X-ray scattering (AXS) experiments to experimentally clarify the structural changes, including partial atomic arrangements by cryogenic rejuvenation [5]. We observed clear structural changes in the nearest-neighbor range and partial atomic movements of Co from the first- to second-nearest neighbor shells. Structural changes in $Gd_{65}Co_{35}$ MG by cryogenic rejuvenation should affect the electronic structures. We have investigated the changes in electronic structures by photoemission and inverse-photoemission spectroscopies (PES and IPES) as well as soft X-ray absorption and emission spectroscopies (SXAS and SXES). Among them, we presented the results of IPES below. Figure 1(a) shows the IPES results before (blue) and after (red) the cryogenic rejuvenation. As seen in the figure, the spectra show large and small peaks at about 6 and 17 eV, respectively, and the first peak shifts towards the lower energy by the rejuvenation [6], and this peak is probably composed of Co 3*d* partial density of states (pDOS).

Subsequently, we tried to find if the above changes by cryogenic rejuvenation can be adopted universally over MGs and to examine the relationship between the structural heterogeneity and electronic changes. In this report, we exhibit the result on $Dy_{65}Ni_{35}$ MG to show the universality of the changes in electronic states in rare earth-transition metal MGs [7].

The $Dy_{65}Ni_{35}$ MG sample was manufactured at Tohoku University by a splat quenching method using a single Cu roll from molten mixture under high purity He atmosphere. A thermal cycling treatment was carried out by soaking the sample into liquid N_2 at 77 K and liquid methanol at about room temperature in steps of 1 min each with the number of times of 40. The IPES experiments were carried out at the resonant IPES spectroscopy (RIPES) station in the Hiroshima Research Institute for Synchrotron Radiation Science. The self-developed IPES spectrometer is equipped with a low-energy electron gun, a non-periodic spherical grating, and a one-dimensional photon detector. The total energy resolution was ~0.5 eV at the electron gun energy E_k of 50 eV. The energy of the IPES spectra is referred to E_F, determined from the Fermi edge of the IPES spectra of an Au film. All the IPES experiments were carried out at room temperature. Clean surfaces

were in situ obtained by scraping the samples with a diamond file in a sample preparation chamber attached with the analyzer one, both of which were kept under ultrahigh vacuum below 1×10^{-8} Pa.

Figure 1(b) shows the IPES spectra of $Dy_{65}Ni_{35}$ MG before (blue) and after (red) the temperature cycling. As seen in the figure, the difference between the spectra before and after the rejuvenation is quite small compared with those of $Gd_{65}Co_{35}$ MG where a large shift of the first peak towards the lower energy is observed as shown in Fig. 1(a). Nevertheless, a shoulder at about 9 eV becomes slightly larger by the cryogenic rejuvenation.

In addition to these works, we measured PES, SXAS, and SXES performed near the Ni 2*p*-3*d* resonances, and the 3*d* pDOS are obtained [7]. The results are under analyzing. Moreover, an *ab-initio* molecular dynamics simulation is planned to obtain further information on the atomic and electronic changes by the cryogenic rejuvenation on the rare earth-TM glasses.

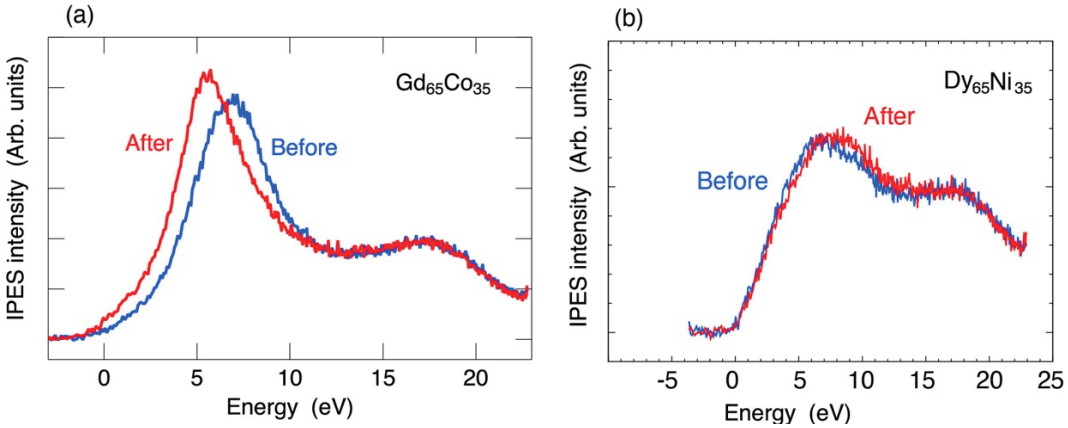

FIGURE 1. IPES spectra of (a) $Gd_{65}Co_{35}$ [6] and (b) $Dy_{65}Ni_{35}$ MGs before (blue) and after (red) cryogenic rejuvenation.

This work was supported by the Japan Society for the Promotion of Science (JSPS) Grant-in-Aid for Transformative Research Areas (A) 'Hyper-Ordered Structures Science' (Nos. 20H05878 and 21H05569), that for Scientific Research (C) (No. 22K12662), and the Japan Science and Technology Agency (JST) CREST (No. JP-MJCR1861).

REFERENCES

1. S. V. Ketov et al., *Nature* **524**, 200-203 (2015).
2. T. C. Hufnagel, *Nat. Mater*. **14**, 867-868 (2015).
3. G. P. Johari, *J. Non-Cryst. Solids* **307-310**, 317-325 (2002).
4. Y. Yamazaki, *Doctoral thesis* (Tohoku University, 2016).
5. S. Hosokawa et al., *Acta Mater*. **284**, 120616-1-10 (2025).
6. S. Hosokawa et al., *Scr. Mater.,* submitted.
7. S. Hosokawa et al., *Acta Mater.,* to be submitted.

Observation of *c-f* hybridization bands of $YbNi_3Ga_9$ by ARPES

Y. Tanimoto[a], M. Sugimoto[a], Y. Nakashima[a], H. Sato[b], M. Arita[b], S. Nakamura[c], S. Ohara[c]

[a]*Graduate School of Advanced Science and Engineering, Hiroshima University, Higashi-Hiroshima 739-8526, Japan*
[b]*Research Institute for Synchrotron Radiation Science, Hiroshima University, Higashi-Hiroshima 739-0046, Japan*
[c]*Graduate School of Engineering, Nagoya Institute of Technology, Nagoya 466-8555, Japan*

Keywords: *c-f* hybridization, angle-resolved photoemission spectroscopy

Trigonal $YbNi_3Ga_9$ crystallizes in the trigonal $ErNi_3Al_9$-type structure with space group R32. While $YbNi_3Al_9$, which has the same structure and a similar valence electron count, exhibits a chiral magnetic order [1], $YbNi_3Ga_9$ is a valence-fluctuating system without long-range magnetic order [2]. In $YbNi_3Ga_9$, strong hybridization between Yb 4*f* and conduction electrons (*c-f* hybridization) is expected. In this study, we performed angle-resolved photoemission spectroscopy (ARPES) on $YbNi_3Ga_9$ to probe the *c-f* hybridized bands. The measurements were carried out at beamline BL-9A of the Research Institute for Synchrotron Radiation Science, Hiroshima University.

Figure 1 presents the ARPES intensity plots of $YbNi_3Ga_9$ measured at $h\nu$ = 24 eV with *p* -polarized geometry along the $\bar{\Gamma}$-$\bar{M}$ direction of the surface Brillouin zone. An almost flat band associated with the Yb^{2+} $4f_{7/2}$ state is observed at 0.07 eV, while several dispersive bands around the Γ point are attributed to conduction-electron states. Notably, the bands exhibit upward and downward splitting at the crossing points between the Yb 4*f* and conduction-electron bands, indicating strong *c-f* hybridization in $YbNi_3Ga_9$. A qualitative estimation of the *c-f* hybridization energies, based on a periodic Anderson model neglecting Coulomb interactions between 4*f* electrons, is currently in progress.

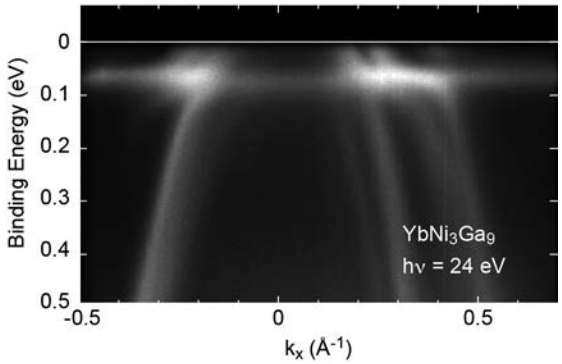

FIGURE 1. ARPES image of $YbNi_3Ga_9$ measured along $\bar{\Gamma}$-$\bar{M}$ directions at $h\nu$=24 eV with *s*-polarized geometry.

REFERENCES

1. S. Ohara, S. Fukuta, K. Ohta, H. Kono, T. Yamashita, Y. Matsumoto and J. Yamaura, JPS Conf. Proc. **3**, 017016 (2014).
2. Y. Utsumi, H. Sato, S. Ohara, T. Yamashita, K. Mimura, S. Motonami, K. Shimada, S. Ueda, K. Kobayashi, H. Yamaoka, N. Tsujii, N. Hiraoka, H. Namatame and M. Taniguchi, Phys. Rev. B **86**, 115114 (2012).

Effects for the Electronic Structure by Oxygen Deficiency on the double-layer Cuprate High-T_c Superconductor, Bi2212

K. Kawamoto[a], H. Yamaguchi[b], Y. Miyai[b], Y. Onishi[b], M. Arita[c], K. Shimada[b,c,d,e], and S. Ideta[b,c]

[a] *Faculty of Science, Hiroshima Univ., Higashi-Hiroshima 739-8526, Japan*
[b] *Graduate School of Advanced Science and Engineering, Hiroshima Univ., Higashi-Hiroshima 739-8526, Japan*
[c] *Research Institute for Synchrotron Radiation Science (HiSOR), Hiroshima Univ., Higashi-Hiroshima 739-0046, Japan*
[d] *Research Institute for Semiconductor Engineering, (RISE), Hiroshima Univ., Higashi-Hiroshima 739-8527, Japan*
[e] *International Institute for Sustainability with Knotted Chiral Meta Matter (WPI-SKCM^2), Higashi-Hiroshima 739-8526, Japan*

Keywords: high-T_c cuprate superconductors, electronic structure, ARPES

Cuprate superconductors have been one of the materials which show the highest superconducting transition temperature (T_c) in superconductors under atmosphere. To elucidate the microscopic mechanism of the high T_c in cuprates; however, it has been unclear so far regardless of a lot of intensive studies [1]. Among Bi-based high-T_c cuprates, a double layer cuprate, $Bi_2Sr_2CaCu_2O_{8+\delta}$ (Bi2212) is a representative material which shows high-T_c superconductivity [2]. T_c and the electronic structure of cuprates dramatically changes with carrier doping, and therefore, one needs to understand the mechanism about these trends to achieve a higher T_c in superconductors.

According to the recent experimental study of Bi2212 using angle-resolved photoemission spectroscopy (ARPES), with increasing the hole carrier, the shape of the electronic structure shows a sudden discontinuous change around a hole doping level (p_c) of ~ 0.19 [3]. Therefore, the previous study suggests that the phase transition occurs at $p_c \sim 0.19$, but the origin of the phase transition has not been clear yet.

To investigate the electronic structure change with changing hole carrier, we have performed the temperature dependent ARPES study for two different Bi2212 samples with $p \sim 0.17$ and ~ 0.22. The ARPES spectra shows different shape compared with the previous results [3]. One of the unexpected features is that the peak-dip-hump structure at 20 K and 60 K, which was observed in the previous study, is not observed in the present experiment.

In this poster presentation, we will show the temperature dependent ARPES spectra in details and discuss the origin of the phase transition at $p_c \sim 0.19$.

REFERENCES

1. A. Damascelli *et al*., Rev. Mod. Phys. 75, 473 (2003).
2. H. Eisaki *et al*., Phys. Rev. B 69, 064512 (2004).
3. S. D. Chen *et al*., Science **366**, 1099-1102 (2019).

Spin-resolved photoemission spectroscopy of chiral magnet $Yb(Ni_{1-x}Cu_x)_3Al_9$

Y. Tanimoto[a], Y. Nakashima[a], K. Kimura[a], H. Sato[b], K. Sumida[b], K. Miyamoto[b], T. Okuda[b], S. Nakamura[c], S. Ohara[c]

[a]*Graduate School of Advanced Science and Engineering, Hiroshima University, Higashi-Hiroshima 739-8526, Japan*
[b]*Research Institute for Synchrotron Radiation Science, Hiroshima University, Higashi-Hiroshima 739-0046, Japan*
[c]*Graduate School of Engineering, Nagoya Institute of Technology, Nagoya 466-8555, Japan*

Keywords: chiral magnet, spin-resolved angle resolved photoemission spectroscopy

Trigonal $YbNi_3Al_9$ has a chiral crystal structure belonging to the space group *R*32 (No. 155) and is notable as the first chiral magnetic alloy discovered among 4*f*-electron compounds [1]. The localized Yb 4*f* moments order magnetically below $T = 3.4$ K, exhibiting ferromagnetism in the ab-plane and forming left- or right-handed helical structures with a propagation vector $\boldsymbol{q} = (0, 0, 0.8)$ [2]. Substitution of Ni with Cu significantly enhances the magnetic interaction, reducing the propagation vector to $\boldsymbol{q} = (0, 0, 0.4)$ in $Yb(Ni_{0.94}Cu_{0.06})_3Al_9$. This behavior is attributed to spin-polarized conduction electrons.

In this study, we performed spin-resolved photoemission spectroscopy (SRPES) on $YbNi_3Al_9$ and $Yb(Ni_{0.94}Cu_{0.06})_3Al_9$. Single crystals for SRPES measurements were grown by the flux method [3]. The experiments were carried out at beamline BL-9B (ESPRESSO end station [4]) of the Research Institute for Synchrotron Radiation Science, Hiroshima University.

Figure 1(a) shows the spin-integrated angle-resolved photoemission spectra (ARPES) of $Yb(Ni_{0.94}Cu_{0.06})_3Al_9$ measured at $h\nu$ = 24 eV with *s*-polarized geometry along the $\bar{\Gamma}$-$\bar{M}$ direction of the surface Brillouin zone at 10 K. Two prominent hole-like bands, labeled A and B, are clearly observed. SRPES spectra were measured for both bands.

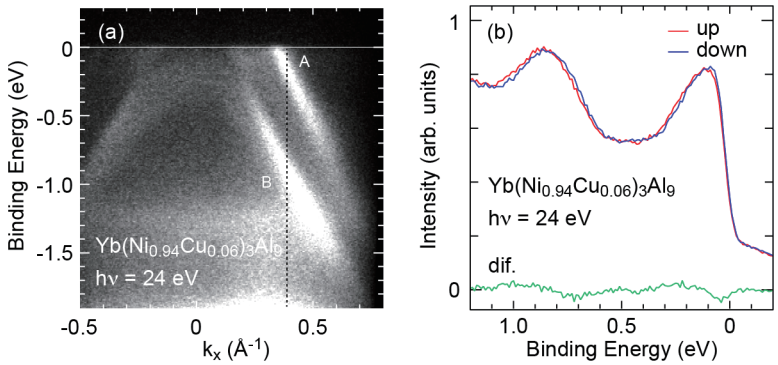

FIGURE 1. (a) ARPES image of $Yb(Ni_{0.94}Cu_{0.06})_3Al_9$ measured along $\bar{\Gamma}$-$\bar{M}$ directions at $h\nu$=24 eV with *s*-polarized geometry. (b) In-plane ($\bar{\Gamma}$-$\bar{K}$ direction) spin-resolved energy distribution (EDC) curves along a cut as indicated by a dashed line in Fig. 1 (a). The difference spectrum is also shown.

Figure 1(b) presents in-plane ($\bar{\Gamma}$-$\bar{K}$ direction) spin-resolved energy distribution curves (EDCs), taken along the cut indicated by the dashed line in Fig. 1(a). The red and blue curves correspond to spin-up and spin-down components, respectively. The structure just below the Fermi level corresponds to band A, while the feature around 0.85 eV is associated with band B. The difference spectrum, also shown in the figure, indicates that the spin-up component is slightly shifted toward higher binding energy. This shift is reflected

in the difference spectrum, providing evidence for spin splitting in bands A and B. Further high-precision measurements are required to confirm these findings.

REFERENCES

1. S. Ohara, S. Fukuta, K. Ohta, H. Kono, T. Yamashita, Y. Matsumoto and J. Yamaura, JPS Conf. Proc. **3**, 017016 (2014).
2. T. Matsumura, Y. Kita, K. Kubo, Y. Yoshikawa, S. Michimura, T. Inami, Y. Kousaka, K. Inoue and S. Ohara, J. Phys. Soc. Jpn. **86**, 124702 (2017).
3. T. Yamashita, R. Miyazaki, Y. Aoki and S. Ohara, J. Phys. Soc. Jpn. **81**, 034705 (2012).
4. T. Okuda, K. Miyamoto, H. Miyahara, K. Kuroda, H. Namatame and M. Taniguchi, Rev. Sci. Instrum. **82**, 103302 (2011).

Anisotropic Topological Surface States Induced by One-Dimensional Structure and Their Thickness Dependence

R. Yamamoto[a], Y. Fujisawa[b], K. Sumida[b], H. Sato[b], K. Miyamoto[b],

and T. Okuda[b,c,d].

[a]*Graduate School of Advanced Science and Engineering Hiroshima University, 1-3-1 Kagamiyama Higashi-Hiroshima 739-8526, Japan*
[b]*Research Institute for Synchrotron Radiation Science (HiSOR), Hiroshima University, 2-313 Kagamiyama, Higashi-Hiroshima 739-0046, Japan*
[c]*International Institute for Sustainability with Knotted Chiral Meta Matter (WPI-SCKM2), Hiroshima University, 2-313 Kagamiyama, Higashi-Hiroshima 739-0046, Japan*
[d]*Research Institute for Semiconductor Engineering (RISE), Hiroshima University, 1-4-2 Kagamiyama, Higashi-Hiroshima 739-8527, Japan*

Keywords: Topological Surface States, Silicon Vicinal Surface, Anisotropy of Band Structure, Bi_2Te_3 film

Topological insulators have spin-polarized metallic surface states called topological surface states (TSS). As in the Fig. 1(a), in the TSS, the spin direction of electrons is locked by their momentum resulting the helical spin-texture. The unique helical spin-texture is considered to prohibit complete backscattering by non-magnetic impurities. This property is expected to realize long spin coherent length and applied for spintronics devices. However, other backscattering passes except for the complete backscattering are not prohibited completely [Fig.1(a)]. One solution to overcome this problem is to form an anisotropic TSS, ideally a one-dimensional TSS [Figs. 1(b) and 1(c)] in which the direction of spin becomes closer to anti-parallel at the opposite k-point.

In the previous research, it has been reported that a quasi-one-dimensional band structure can be realized in the Ag films on Si(111)-(4 × 1)-In surface in which Ag film has regular step and terrace structure [1]. Thus, we expected that a similar effect might occur in the topological insulator film on vicinal surface with atomically regular step arrays. To investigate this hypothesis, we tried to fabricate Bi_2Te_3 film on silicon vicinal surface and measure its electronic structure.

Bi_2Te_3 ultrathin films were grown by molecular beam epitaxy on Si(111) and Si(557), which were used as a flat and a vicinal surface substrate, respectively. Si(557) is a surface tilted by 9.5° from Si(111), and has a Si(111) plane with a terrace width of 1.8 nm. The qualities of these films are evaluated by low energy electron diffraction (LEED) and auger electron spectroscopy (AES). Figure 2 shows LEED pattern and AES spectrum of the Bi_2Te_3 film on each substrate. As in Fig. 2(b) and (d), we can see clear spots in LEED and peak of Bi and Te in AES indicating that we succeeded in growing the Bi_2Te_3 film on both surfaces.

To observe the band structure of the fabricated films, angle-resolved photoemission spectroscopy (ARPES) measurements were performed at BL-9B in HiSOR using He Iα (21.2 eV) light. Figure 3(a), (b) shows the Fermi surface (top) and band structure (bottom) of 5 quintuple layer (QL) Bi_2Te_3 film on Si(557) surface. In these results, we can see the anisotropic TSS and Dirac point at around – 0.4 eV, which indicates that TSS is expanded to the direction perpendicular to the step by the effect of electron confinement. Figure 3(c), (d) and Figure 3(e), (f) show the results of 1~2 QL sample and less than 1 QL sample, respectively. In Figure 3(c), (d), we can see the anisotropic Fermi surface, but in Figure 3(e), (f), the anisotropy of Fermi surface and band structure is much weaker compared to 1~2 QL sample. Additionally, comparing the elongation of the Fermi surface, Fig. (c) (1~2 QL sample) shows the strongest anisotropy. This means the band anisotropy induced by evaporating on vicinal surface depends on the film thickness and quality of

substrate.

In conclusion, we succeeded in growing the Bi_2Te_3 film on vicinal silicon surface and observing the anisotropic topological surface states. In addition, we could also investigate the properties of the thin film on the vicinal surface. From these results, we found that it is possible to fabricate the one-dimensional topological insulator. Additionally, to effectively utilize the spin-texture of the anisotropic TSS, controlling the film thickness and ensuring the quality of substrate are important. These results will contribute to realizing the long spin coherent length and the future spintronics applications.

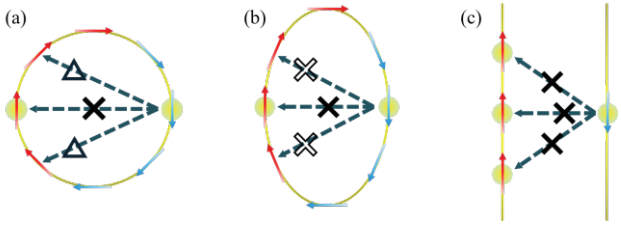

FIGURE 1. Schematic spin-texture of (a) isotropic, (b) anisotropic, and (c) one-dimensional Fermi surfaces (c) of topological insulators.

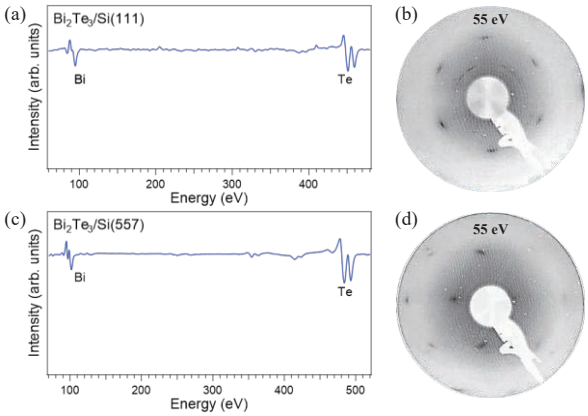

FIGURE 2. (a) AES spectrum of Bi_2Te_3/Si(111) (b)LEED pattern of Bi_2Te_3/Si(111) taken at 55 eV. (c),(d) the same as (a), (b) but of Bi_2Te_3/Si(557)

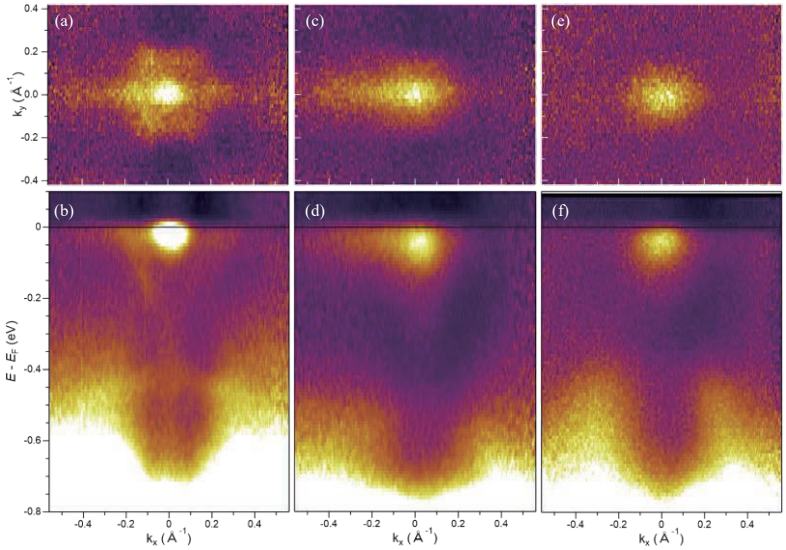

FIGURE 3. (a) Fermi surface and (b) band structure of 5 QL Bi_2Te_3/Si(557). (c), (d) the same as (a), (b) but of 1~2 QL Bi_2Te_3/Si(557). (e), (f) the same as (a), (b) but of less than 1 QL Bi_2Te_3/Si(557). All the data were measured by He Iα (21.2 eV) light.

REFERENCES

1. N. Nagamura *et al.*, Phys. Rev. Lett. **96**, 256801 (2006).
2. S. Hatta *et al.*, Sci. Rep. **11**, 5742 (2021).

Oxygen-termination effect of the spin-dependent electronic states in FeCo/Rh(001) thin film

Kaori Kunitomo[a], Kazuki Sumida[b], Koji Miyamoto[b], and Taichi Okuda[b,c,d]

[a] *Graduate School of Advanced Science and Engineering Hiroshima University, 1-3-1 Kagamiyama, Higashi-Hiroshima, 739-8526 Japan*
[b] *Research Institute for Synchrotron Radiation Science (HiSOR), Hiroshima University, 2-313 Kagamiyama, Higashi-Hiroshima, 739-0046 Japan*
[c] *International Institute for Sustainability with Knotted Chiral Meta Matter (WPI SKCM2) Hiroshima University, 2-313 Kagamiyama, Higashi Hiroshima, 739-0046 Japan*
[d] *Research Institute for Semiconductor Engineering (RISE) Hiroshima University, 1-4-2 Kagamiyama, Higashi-Hiroshima, 739-8527 Japan*

Keywords: FeCo thin films, perpendicular magnetic anisotropy, VLEED spin detection target, oxygen termination

The emergence of perpendicular magnetic anisotropy (PMA) in magnetic thin films is essential from a practical application standpoint, as it contributes to increasing the recording density of storage devices and reducing energy consumption. Many magnetic thin films exhibiting PMA, such as Co/Pt, Co/Pd, FePt, TbFeCo, and GdFeCo, have been extensively investigated. Among them, FeCo alloy films, which are free of rare-earth and noble-metal elements, are considered promising candidates exhibiting strong PMA. Burkert *et al*. predicted that the magnetic anisotropy energy may increase in FeCo alloys when the tetragonal distortion is applied [1]. Specifically, at a *c*/*a* ratio of approximately 1.20-1.25, the magnetic anisotropy energy exceeds 700-800 μeV/atom, which is one or two orders of magnitude greater than that of pure Fe or Co. The emergence of strong PMA was experimentally confirmed in tetragonally distorted FeCo ultra-thin films grown on Rh(001) (*c*/*a* = 1.24) with a thickness of 13-15 monolayers (ML) [2].

Furthermore, the FeCo thin films exhibiting PMA could be useful as a target for out-of-plane spin component in very low energy electron diffraction (VLEED) spin detectors [3,4]. In the present VLEED spin detector, Fe(001)*p*(1×1)-O films, which exhibit in-plane magnetic anisotropy and can detect only in-plane spin components (P_x, P_y), are widely used. However, to observe all components of spin polarization (P_x, P_y, P_z) with the VLEED detectors, a ferromagnetic thin film target with PMA is required in addition to the conventional Fe(001)*p*(1×1)-O films. Moreover, Fe(001)*p*(1×1)-O has an oxygen-adsorbed overlayer that serves as a protection layer from further oxidization and contamination, extending its lifetime from hours to weeks (or even several months or more with flash annealing). Thus, if the preparation method of oxygen-adsorbed protection layer on FeCo films is established, the FeCo-O films may be usable for long-term use as the VLEED targets for the out-of-plane spin component.

In this study, we fabricated the oxygen-terminated FeCo films on a Rh(001) single-crystal substrate and investigated the spin-polarized electronic structures and their lifetime utilizing spin- and angle-resolved photoemission spectroscopy (SARPES).

The samples were fabricated by using two different methods. In the first method, after cleaning the Rh(001) substrate by cycles of 2 keV Ar^+-ion sputtering and subsequent annealing at 1000 ˚C, FeCo was deposited at room temperature. Then, the FeCo film was exposed to approximately 30 L of oxygen and post-annealed at 300° C for 5 min. As a result, the low energy electron diffraction (LEED) pattern shows not only the 1×1 spots but also new superlattice spots [Fig. 1(b)]. Furthermore, while a clear out-of-plane spin polarization was observed at the pristine FeCo thin film [Fig. 2(a)], the spin polarization was almost diminished after oxygen exposure [Fig. 2(b)], indicating the loss of PMA.

Next, we explored a second method in which oxygen was introduced prior to the FeCo deposition, aiming to induce oxygen segregation. Specifically, after cleaning the Rh(001) substrate, oxygen exposure was exposed ~30 L to the substrate, followed by FeCo deposition and post-annealing at 300° C for 5 min. In this method, we obtained clear 1×1 LEED spots [Fig. 1(c)] similar to that of the pristine FeCo film [Fig. 1(a)].

More importantly, we observed a distinct out-of-plane spin polarization [Fig. 2(c)]. These results indicate that the FeCo thin film successfully retained perpendicular magnetic anisotropy even after oxygen termination.

Finally, to evaluate the protection effect of oxygen termination, we monitored the spin-polarization of both pristine FeCo and oxygen-terminated FeCo thin films over approximately one week. Figure 3 shows the time-dependent spin-polarization. Here, we estimated the time constant for an attenuation of out-of-plane spin-polarization, *i.e.* lifetime, by fitting the experimental results with an exponential function. As a result, the time constant of the oxygen-terminated FeCo thin film was approximately 5.5 times longer than that of the pristine FeCo thin film. This finding suggests that, similar to Fe(001)$p(1\times1)$-O, the oxygen termination provides an effective surface protection effect for FeCo thin films.

Based on these results, oxygen-terminated FeCo thin films appear to be highly promising as targets for out-of-plane spin component in VLEED spin detector.

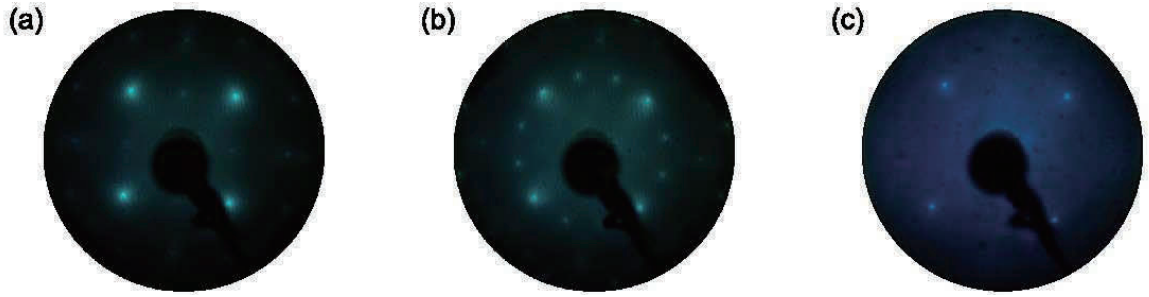

FIGURE 1. LEED patterns of the pristine FeCo thin film (a) and the oxygen-exposed FeCo film fabricated by the methods I (b) and II (c) taken at 90 eV.

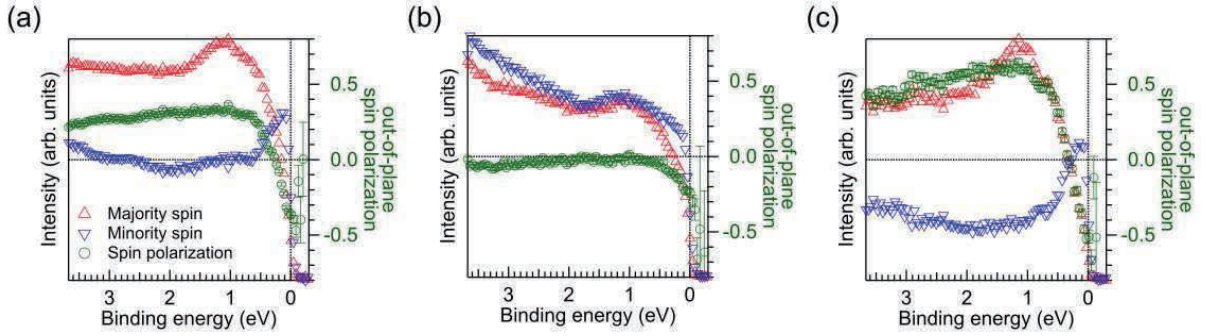

FIGURE 2. Out-of-plane spin-resolved photoemission spectra taken at 21.2 eV (He discharge lamp). The samples correspond to those in Fig. 1. A magnetic field was applied in the out-of-plane direction prior to the measurement. Red (blue) represents the majority (minority) spin, and green represents the out-of-plane spin polarization.

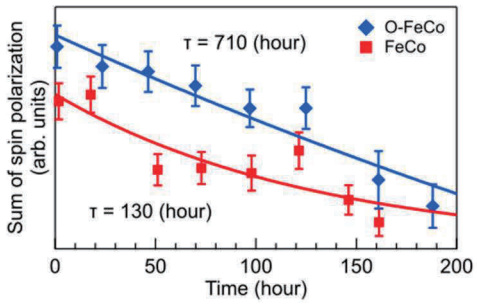

FIGURE 3. Comparison of the time constant for an attenuation of out-of-plane spin polarization. Red (blue) represents FeCo thin film (oxygen-terminated FeCo thin film).

REFERENCES

1. T. Burkert *et al.*, Phys. Rev. Lett. **93**, 027203 (2004).
2. F. Yildiz *et al.*, Phys. Rev. B **80**, 064415 (2009).
3. T. Okuda *et al.*, Rev. Sci. Instrum. **79**, 124117 (2008).
4. T. Okuda *et al.*, Rev. Sci. Instrum. **82**, 103302 (2011).

Spin-Polarized Polarons in Surface-Doped Tungsten Disulfides

Changmo Kang[a], Yoonseok Oh[a], Seungkyu Park [a], and Keun Su Kim[a]

[a]*Department of Physcis, College of Science, Yonsei University, Seoul Korea*

Keywords: ARPES, spin-resolved photoemission, polarons, WS_2, electron-phonon coupling.

Understanding how charge carriers interact with the lattice is crucial for decoding the low-energy physics of quantum materials. Among various many-body excitations, polarons represent a key concept in describing charge transport, mass renormalization, and spectral reconstruction. Surface doping in layered materials provides a unique pathway to study polaronic quasiparticles, as it allows for systematic tuning of the carrier density while preserving the two-dimensional character of the host system. Angle-resolved photoemission spectroscopy (ARPES) has been instrumental in capturing such effects, as evidenced in TiO_2, $SrTiO_3$, and more recently MoS_2, where characteristic replica bands and quasiparticle renormalizations consistent with Holstein or Fröhlich-type polarons have been reported.

Building on this prior knowledge, our study focused on WS_2, a transition metal dichalcogenide with strong intrinsic spin-orbit coupling (SOC). The presence of SOC, combined with inversion symmetry breaking at the surface, gives rise to spin-split electronic states via the Rashba effect, especially near the T point in the Brillouin zone. While previous ARPES measurements have identified multiple polaronic replicas in surface-doped WS_2, the spin character of these replicas remained unexplored. If these replicas arise from spin-split initial states, as predicted, they could inherit spin polarization, thereby revealing a new class of spin-polarized many-body quasiparticles — a concept with profound implications for spintronics and polaron physics.

To investigate this hypothesis, we carried out spin-resolved ARPES experiments at the BL-9B beamline of HiSOR, one of the few facilities worldwide offering synchrotron-based spin-ARPES with sufficient energy resolution and photon flux. The experiment was carefully designed to match the conditions of previous spin-integrated measurements for consistency. High-quality single crystals of WS_2 were cleaved in situ under ultra-high vacuum conditions (~10^{-11} Torr) to expose pristine surfaces. Surface doping was achieved by in situ evaporation of rubidium using a custom-built evaporator system brought from Yonsei University, which was fully compatible with the BL-9B chamber infrastructure.

We used photons in the range of 40–60 eV to access both the T and K points in momentum space with sufficient resolution and momentum reach. Sample temperatures were kept below 15 K to minimize thermal broadening and enhance the visibility of weak features. The first day was dedicated to reproducing the previously observed polaronic replicas and optimizing doping conditions. Once the characteristic Holstein satellite bands were clearly identified, we performed spin-resolved measurements using a Mott-type spin detector integrated into the analyzer system.

Our data revealed two key findings. First, at the T point, the electronic states exhibited Rashba-type spin splitting, consistent with theoretical expectations and prior spin-integrated measurements. Second, and more crucially, at the K point — where the main quasiparticle peak was largely suppressed at low doping — the satellite features displayed a finite, reproducible spin asymmetry. This suggests that these polaronic satellites originate from spin-polarized states and retain spin information even after strong many-body renormalization.

This is a significant result. It implies that spin-polarized Holstein polarons can exist in real materials, and their signatures can be directly measured using spin-ARPES. To our knowledge, this is the first experimental evidence of such quasiparticles, bridging the domains of spin physics and strong electron-phonon interaction. These findings open exciting possibilities for realizing spin-dependent transport mediated by polarons and may inspire new theoretical models that incorporate both spin textures and lattice interactions on equal footing.

The results obtained during this beamtime will form the core part of a comprehensive publication currently in preparation. Once finalized, the study will not only conclude a multi-year project combining several ARPES techniques and beamlines but also serve as a cornerstone for future investigations into spin-polarized many-body phenomena in two-dimensional semiconductors.

REFERENCES

1. S. Moser et al., *Phys. Rev. Lett*. 110, 196403 (2013).
2. Z. Wang et al., *Nature Mater.* 15, 835 (2016).
3. M. Kang et al., *Nature Mater.* 17, 676 (2018).

Electronic Structure of Weyl Ferromagnet Co_2MnGa Thin-Film in Ordered and Disordered Phases

Kazuki Sumida[a], Tomohiko Asano[b], Yuya Sakuraba[c], Keisuke Masuda[c], Yuita Fujisawa[a], Koji Miyamoto[a], Akio Kimura[b,d,e,f], and Taichi Okuda[a,d,e]

[a]*Research Institute for Synchrotron Radiation Science (HiSOR), Hiroshima University, 2-313 Kagamiyama, Higashi-Hiroshima, Hiroshima, Japan.*
[b]*Graduate School of Advanced Science and Engineering, Hiroshima University, 1-3-1 Kagamiyama, Higashi-Hiroshima, Hiroshima, Japan.*
[c]*Research Center for Magnetic and Spintronic Materials (CMSM), National Institute for Materials Science (NIMS), Sengen 1-2-1, Tsukuba, Ibaraki, Japan.*
[d]*International Institute for Sustainability with Knotted Chiral Meta Matter (WPI-SKCM^2), Hiroshima University, 1-3-1 Kagamiyama, Higashi-Hiroshima, Hiroshima, Japan.*
[e]*Research Institute for Semiconductor Engineering (RISE), Hiroshima University, 1-4-2 Kagamiyama, Higashi-Hiroshima, Hiroshima, Japan.*
[f]*Synchrotron Radiation Research Center, National Institutes for Quantum Science and Technology (QST), 1-1-1 Koto, Sayo, Hyogo, Japan.*

Keywords: Heusler alloy, Weyl semimetal, ARPES.

Weyl ferromagnets possess a topologically nontrivial electronic structure characterized by Weyl cones, which generate a large Berry curvature. This gives rise to gigantic transverse transport properties such as the anomalous Hall (AHE) and Nernst effects (ANE). Among them, the Heusler alloy Co_2MnGa exhibits one of the largest ANE at room temperature, owing to the presence of multiple spin-polarized Weyl cones near the Fermi energy (E_F) [1-3]. More recently, it has been reported that the AHE in Co_2MnGa thin films is strongly influenced by the degree of atomic ordering, with the anomalous Hall conductivity being drastically reduced in the disordered phase [4,5]. However, the detailed differences in the electronic structures between ordered and disordered phases remain unclear, and their relationship to transport properties is not yet fully understood. To address this issue, we experimentally investigated the electronic structure across the order-disorder transition in Co_2MnGa thin films by means of angle-resolved photoelectron spectroscopy (ARPES) with synchrotron radiation.

Co_2MnGa epitaxial thin films with a buffer layers of Cr and Ag were deposited on a MgO(001) single crystalline substrate at room temperature using a co-sputtering technique with Co, Mn, and $Co_{41.2}Mn_{27.5}Ga_{31.3}$ sputtering targets. The Co_2MnGa films were designed to be 30 nm thick. To obtain $L2_1$ ordered and $B2$ disordered phases [Figs. 1(a,b)], the samples were annealed at 550°C and 400°C, respectively. X-ray diffraction (XRD) measurements revealed that a 111 superlattice peak, which characterizes the $L2_1$ ordered phase, was absent in the sample annealed at 400°C, whereas a clear 111 peak was observed in the sample annealed at 550°C [Fig. 1(c)]. ARPES measurements were carried out at the ESPRESSO end-station (BL-9B) in the Research Institute for Synchrotron Radiation Science (HiSOR) [6,7]. The photoelectrons were acquired using a hemispherical electron analyzer (R4000-WAL, Scienta-Omicron). The energy and angular resolutions were set to 60 meV and ±0.3°, respectively. The sample temperature was maintained at 30 K during the measurements.

To determine the high-symmetry points along the k_z direction, photon-energy-dependent ARPES spectra were first acquired in the range $h\nu$ = 50-120 eV with 2.5 eV steps. By comparing the experimental results with band structure calculations, the inner potential was determined to be 14.5 eV. Figures 2(b) and 2(c) present ARPES images of $L2_1$ ordered and $B2$ disordered Co_2MnGa thin films along the K-Γ-K line. In the $L2_1$ ordered phase, metallic bands crossing E_F are clearly visible near the K and Γ points [Fig. 2(b)], in good agreement with the band structure calculations [Fig. 2(a)]. In particular, the bands near the K point are attributed to majority-spin-polarized Weyl cones, which generate a large Berry curvature. In contrast,

although Weyl cones are still discernible near the K point in the *B*2 disordered phase, the bands are significantly broadened, indicating a marked reduction in quasiparticle lifetime [Fig. 2(c)]. These experimental observations are consistent with theoretical calculations based on the KKR-CPA method (not shown), supporting the conclusion that broadening of Weyl cones is responsible for the suppression of transverse transport properties.

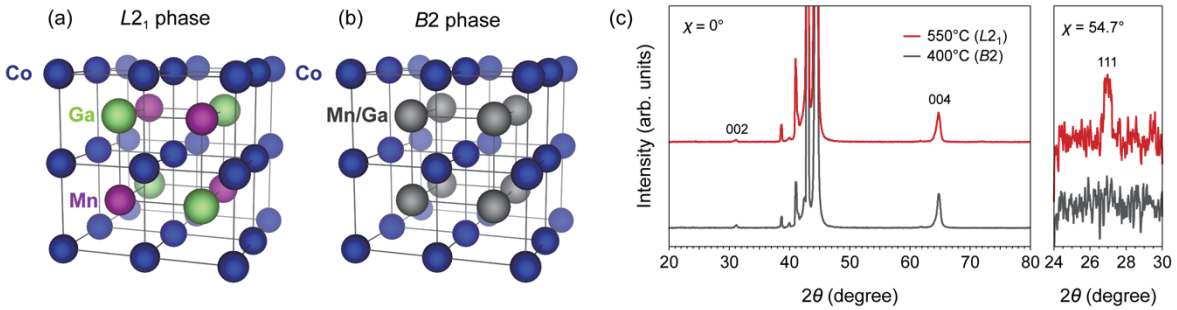

FIGURE 1. (a,b) Crystal structures of Co_2MnGa Heusler alloy in $L2_1$ ordered and *B*2 disordered phases. (c) XRD patterns taken at [001] (left) and [111] (right) directions.

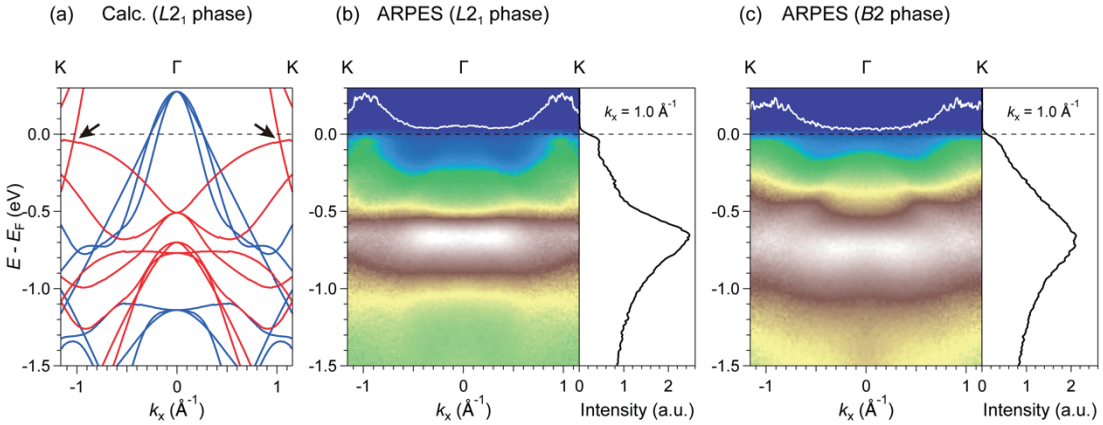

FIGURE 2. (a) Calculated band structure of $L2_1$ ordered Co_2MnGa along the K-Γ-K line. Red (blue) indicates the majority-spin (minority-spin) component. Black arrows indicate the Weyl nodes. (b,c) Experimentally observed band structure of $L2_1$ ordered and *B*2 disordered Co_2MnGa thin films along the K-Γ-K line. ARPES images are symmetrized with respect to the Γ point. White curves represent the momentum distribution curves at E_F. Right panels show the energy distribution curves at k_x = 1.0 Å^{-1}.

REFERENCES

1. A. Sakai *et at*., Nat. Phys. **14**, 1119 (2018).
2. S. N. Guin *et at*., NPG Asia Mater. **11**, 16 (2019).
3. K. Sumida *et at*., Commun. Mater. **1**, 89 (2020).
4. Q. Wang *et al*., Appl. Phys. Lett. **115**, 252401 (2019).
5. Z. Zhu *et al*., AIP Advances **10**, 085020 (2020).
6. T. Okuda *et al*., Rev. Sci. Instrum. **82**, 103302 (2011).
7. T. Okuda *et al*., J. Electron Spectrosc. Relat. Phenom. **201**, 23 (2015).

Study of attosecond photoemission dynamics through photoelectron spin interference effect

Kenta Kuroda[a, b, c], T. Kosa[a], T. Iwata[a, b],
A. Kimura[a, b, c], K. Miyamoto[d], T. Okuda[b, c, d], Y. Koichiro[e], F. Komori[f]

[a]*1Graduate School of Advanced Science and Engineering, Hiroshima University, Japan*
[b]*WPI-SKCM², Hiroshima University, Japan*
[c]*Research Institute for Semiconductor Engineering, Hiroshima University, Japan*
[d]*HiSOR, Hiroshima University Japan*
[e]*Research Center for Advanced Measurement and Characterization, NIMS, Japan*
[f]*Institute of Industrial Science, The University of Tokyo, Japan*

Keywords: spin-ARPES, photoemission, ultrafast dyanamics.

The realization of spin-polarized electrons and their manipulation are the main goal in the field of spintronics. A promising way is by utilizing materials with strong spin-orbit coupling (SOC). The representative examples are Rashba systems and topological insulators, at surfaces of which spin-polarized electrons emerge due to antisymmetric SOC under the lack of inversion symmetry. As a consequence of SOC, the different spin and orbitals are entangled, which can be directly probed by spin- and angle-resolved photoemission spectroscopy (spin-ARPES). Since light polarization can select the orbital part of the wave functions, this entanglement allows us to optically control the electron spin, leading to optospintronic functions.

By previous spin-ARPES studies on the surface state of Bi_2Se_3 [1, 2] and Bi(111) [3], it was demonstrated that *p*- or *s*-polarized light can selectively excite spin-polarized photoelectrons with either spin-up or spin-down from the wave function. By using a tilted linear polarization with both *p*- and *s*-polarization components, both spin states are excited simultaneously and interfere in photoelectron states [Fig. 1], which can be seen as a rotation of the spin orientation from the initial helical-spin state [1-3].

While the above experiments greatly facilitate an optical spin manipulation by a proper light polarization, the biggest advantage of looking at this spin interference phenomena is that one can determine a relative phase difference between the two processes (T_p and T_s), excited either by *p*- or by *s*-polarized light [Fig. 1]. Yet, the physical origin of the phase in the spin interference and its interpretation remain unsolved questions.

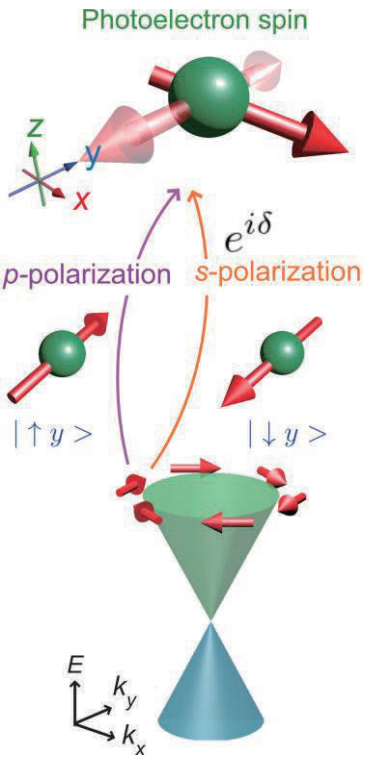

Fig. 1: Superposition of spin-up and spin-down in a photoelectron fina state excited from the Dirac surface state of Bi_2Se_3 [1, 2].

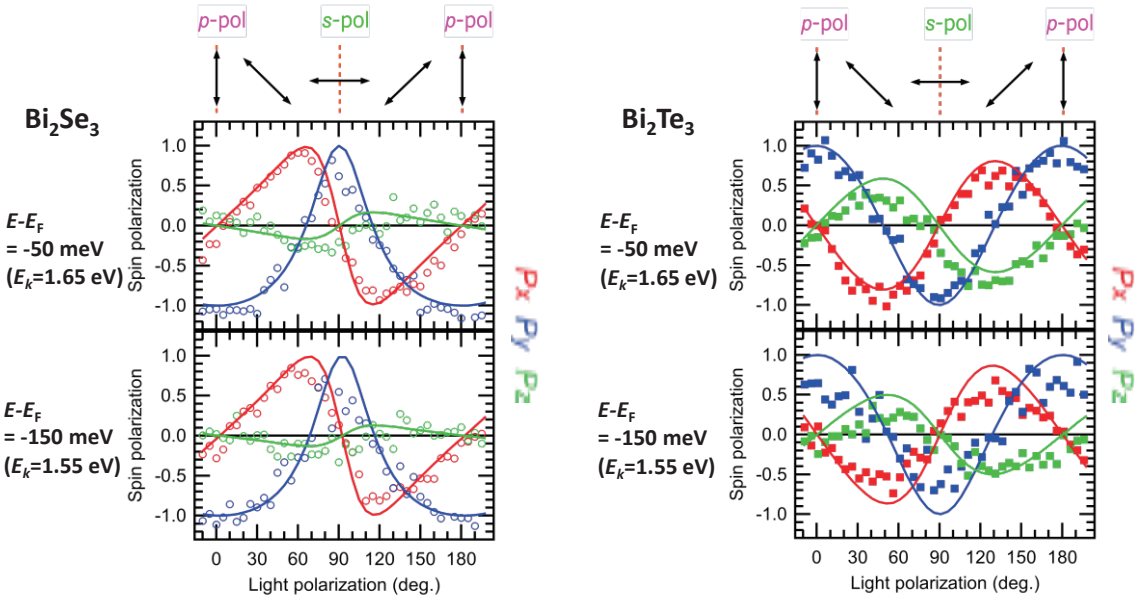

Fig. 2: spin-ARPES results with 6-eV laser at HiSOR [5]. Linear-polarization evolutions of the three-dimensional spin polarization, $P_{x,y,z}$, of the photoelectrons emitted from the surface state of (left) Bi_2Se_3 and (right) Bi_2Te_3.

Fanciulli and Dil *et al* suggested that the phase difference reflects time scale of photoemission dynamics [4]. According to their claim, the phase information, determined by photoemission spectroscopy, can be converted to a delay time of the photoemission processes as follows:

$$\tau = \hbar \left| \frac{\partial \phi}{\partial E_k} \right|$$

where τ, ϕ, and E_k are a delay time, a phase difference, and a kinetic energy of photoelectrons. This formula is obtained by a simplest model, called Eisenbud-Wigner-Smith (EWS) model [4], in which the free electrons scattered by short-range potential are considered and the phase between the incoming and outcoming electrons is shifted. The EWS time is, thus, considered as a sticking time in the interaction potential.

To experimentally determine the kinetic energy dependence of the phase, we used spin-ARPES with 6-eV laser at HiSOR [5] and with 7-eV laser at ISSP [6]. Figures 2(a) and (b) summarize the spin polarization vector of the photoelectrons emitted from the surface state of Bi_2Se_3 and Bi_2Te_3 at two different kinetic energies obtained by laser-SARPES with 6-eV laser. Apparently, the kinetic energy dependence of the spin polarization vector is rather weak, which shows sharp contrast to the results for 7-eV laser-spin-ARPES. This large contradiction between the two independent measurements implies that the spin interference effect is dominated by the final state characters that can be selected by photon energies in photoemission process.

References

[1] Kenta Kuroda, Koichiro Yaji *et al*., Phys. Rev. B **94**, 165162.
[2] Kenta Kuroda, Koichiro Yaji *et al*., Phys. Rev. B **105**, L121106 (2022).
[3] Koichiro Yaji and Kenta Kuroda *et al*., , Nat. Commun. **8**, 14588 (2017).
[4] Mauro Fanciulli *et al*., Phys. Rev. Lett. **118**, 067402 (2017).
[5] Takuma Iwata *et al*., Sci. Rep. **14**, 127 (2024).
[6] Koichiro Yaji *et al*., Rev. Sci. Instrum. **87**, 053111 (2016).

Spin splitting in the surface electronic structure of antiferromagnet NdBi

R. Yamamoto[a,b], T. Motoyama[c], T. Iwata[a,c], T. Kosa[c], Y. Nishioka[c], K. Ideura[c], M. Arita[d], K. Miyamoto[d], T. Okuda[a,d,e], A. Kimura[a,c,e], T. Yamada[f], Y. Yanagi[f], T. Onimaru[c], and K. Kuroda[a,c,e]

[a] *International Institute for Sustainability with Knotted Chiral Meta Matter (WPI-SKCM^2), Hiroshima University, Japan*
[b] *Max Planck Institute for Chemical Physics of Solids, Dresden, Germany*
[c] *Graduate School of Advanced Science and Engineering, Hiroshima University, Japan*
[d] *HiSOR, Hiroshima University, Japan*
[e] *Research Institute for Semiconductor Engineering, Hiroshima University, Japan*
[f] *Liberal Arts and Sciences, Toyama Prefectural University, Japan*

Keywords: antiferromagnetism, spin splitting, band structures, spin-ARPES.

In recent years, antiferromagnets have attracted growing attention as a new platform for studying spin-polarized electrons [1, 2]. Unlike ferromagnets, antiferromagnetic (AFM) materials can exhibit spin splitting even in the absence of net magnetization, due to either time-reversal (T) or inversion (P) symmetry breaking. This phenomenon can be understood from the perspectives of magnetic multipoles [3] and altermagnetism [4]. The emergence of spin-split electronic structures in AFM states has been intensively investigated [5–7]. Furthermore, the AFM order parameter, such as the Néel vector, can function as a state variable for controlling these properties. However, the field of AFM spintronics is still in its early stages, and the difficulty in directly observing spin splitting in AFM states hampers our understanding of how AFM order affects the electronic structure. Rare-earth monopnictides RX (R: rare-earth, X: pnictogen), which crystallize in a NaCl-type structure, have recently gained renewed interest because their electronic structures can be significantly altered by AFM ordering. Angle-resolved photoemission spectroscopy (ARPES) has revealed both the sensitivity of their band structures to AFM configurations and the strong coupling between itinerant carriers and localized 4f electrons [8, 9]. In particular, NdBi exhibits the emergence of surface states and the development of band splitting across the AFM transition at T_N=24 K [10]. Density functional theory (DFT) calculations have suggested that this originates from spin-split surface states formed within a band-folding-induced hybridization gap [11]. So far, the spin information of these states has been inferred only through circular dichroism (CD) in ARPES measurements [10], although CD primarily probes orbital, rather than spin, degrees of freedom [10]. Therefore, spin-resolved ARPES (spin-ARPES) is essential for reliably determining the spin splitting and its momentum-space texture. In this work, we employed laser spin-ARPES at HiSOR [12] to directly probe the spin degrees of freedom in the electronic structure of NdBi in its AFM state.

In this experiment, photoelectrons were detected along a high-symmetry direction using p-polarized light [Fig. 1(d)], ensuring sensitivity to the initial state information. Figure 1(a) shows the ARPES image along the k_x direction in AFM phase, where two surface band dispersions (ss1 and ss2) appear around k_x~0.2 Å^{-1}. These bands were previously interpreted as spin-split counterparts, since the energy separation between ss1 and ss2 increases as the temperature

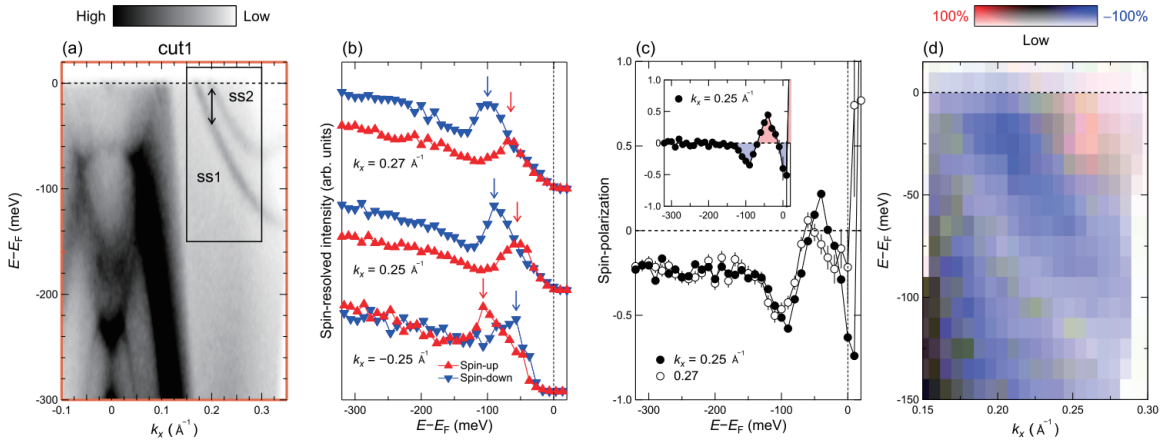

Fig. 1: (a) Band dispersion in the AFM state along k_x. Double arrow represents energy gap between ss1 and ss2. (b) Laser-SARPES spectra for the S_y component at representative k_x points, −0.25, 0.25, and 0.27 Å^{-1}. (c) Corresponding spin polarization spectra at k_x=0.25 and 0.27 Å^{-1}. The result after subtracting the spin-polarization background is presented in the inset. (d) Spin-polarization map acquired in the E-k_x window [rectangle denoted in (a)]. The blue-red color corresponds to the size of the spin polarization, and the brightness corresponds to the intensity.

decreases [10]. Thanks to the spin resolution of our laser-SARPES system, we can now access their spin information directly.

Figure 1(b) displays the spin-resolved spectra for the spin component S_y, corresponding to the helical spin direction, at representative k_x values. At k_x=0.25 Å^{-1}, the spin-up and spin-down spectra each exhibit a single peak at different binding energies, as indicated by arrows. A similar trend is observed at k_x=0.27 Å^{-1}, where the peaks are shifted toward lower energies, indicating that our laser spin-ARPES traces both the band dispersion and the spin texture [Fig.1(c) and (d)]. Since ss1 and ss2 correspond to the spin-up and spin-down states, respectively, we conclude that the observed band splitting originates from the lifting of spin degeneracy. One might ask whether the spin splitting of ss1 and ss2 in the AFM state arises from time-reversal T-symmetry breaking or P-symmetry breaking. To address this, we measured laser-SARPES spectra at the opposite momentum, k_x=−0.25 Å^{-1} [bottom panel of Fig. 1(b)]. Compared with the spectra at k_x>0, the spin-up and spin-down peak positions are reversed at k_x=−0.25 Å^{-1}. This antisymmetric behavior with respect to the time-reversal-invariant momentum (k=0) indicates that the spin splitting originates from inversion symmetry breaking. This work has been published in Physical Review Research [13].

References

[1] T. Jungwirth, X. Marti, P. Wadley, and J. Wunderlich, Nature Nanotech. **11**, 231 (2016).
[2] V. Baltz *et al*., Rev. Mod. Phys. **90**, 015005 (2018).
[3] H. Watanabe and Y. Yanase, Phys. Rev. B **98**, 245129 (2018).
[4] L. Šmejkal, J. Sinova, and T. Jungwirth, Phys. Rev. X **12**, 040501 (2022).
[5] Y.-P. Zhu et al, Nature (London) **626**, 523 (2024).
[6] J. Krempaský *et al*., Nature (London) **626**, 517 (2024).
[7] T. Osumi *et al.*, Phys. Rev. B **109**, 115102 (2024).
[8] K. Kuroda *et al.*, Nature Commun. **11**, 2888 (2020).
[9] Y. Arai *et al*, Nature Mater. **21**, 410 (2022).
[10] B. Schrunk *et al*., Nature (London) **603**, 610 (2022).s
[11] L.-L. Wang *et al.*, Commun. Phys. **6**, 78 (2023).
[12] T. Iwata *et al.*, Sci. Rep. **14**, 127 (2024).
[13] R. Yamamoto *et al.*, Phys. Rev. Research **7**, L022005 (2025).

A laser spin-ARPES study of kagome lattice magnets

Yuita Fujisawa[a], Takuma Iwata[b,c], Kenta Kuroda[b,c]

[a] *Research Institute for Synchrotron Radiation Science, Hiroshima university, 2-313, Kagamiyama, Higashi-Hiroshima, Hiroshima, 739-0024, Japan.*
[b] *Graduate School of Advanced Science and Engineering, Hiroshima University, 1-3-1 Kagamiyama, Higashi-Hiroshima, Hiroshima 739-8526, Japan.*
[c] *International Institute for Sustainability with Knotted Meta Matter (WPI-SKCM2) Hiroshima University, 2-313 Kagamiyama, Higashi-Hiroshima, Hiroshima 739-0046, Japan*

Keywords: ferromagnet, spin-ARPES, kagome lattice

In recent years, the fractionalization of quasiparticles arising from strong correlation effects has attracted considerable attention [1,2]. A ferromagnetic material, Fe_3Sn_2, in which Fe atoms form a kagome lattice, has drawn interest as a system where the Dirac dispersion is linked to a giant anomalous Hall effect [3,4]. More recently, the existence of fractional quasiparticles has been suggested in this material [5]. According to that report, hybridization between a shallow electron pocket near the $\bar{\Gamma}$ point and a flat band slightly above the Fermi level (E_F) gives rise to a third quasiparticle state. This fractional quasiparticle emerges only in the vicinity of the Fermi level and exhibits an exceptionally long lifetime. However, the microscopic origin of this state remains under debate. In the present study, we performed spin- and angle-resolved photoemission spectroscopy (SARPES) using a laser light source [6] to gain insight into the origin of this quasiparticle state.

Figure 1a shows a representative ARPES dispersion near $\bar{\Gamma}$. Consistent with the previous study [5], a shallow electron pocket is observed, with its band bottom lying between 50 and 100 meV below E_F. In addition, we observed an even shallower electron pocket, resembling the previously reported fractionalized quasiparticle state. To investigate the spin eigenstate associated with the observed band structure, we carried out spin-resolved energy distribution curve (spin-EDC) measurements at k_F, as indicated in Fig. 1a. As shown in Fig. 1c, a clear spin polarization is observed, primarily along the k_y direction. This is consistent with the in-plane magnetic anisotropy of this material. After the spin-EDC measurements, we acquired another ARPES intensity map (Fig. 1b). In this data, the shallower electron pocket is absent, which may imply that the quasiparticle state exists only near the surface. Additional experiments will be required to confirm the spin polarization of this quasiparticle state.

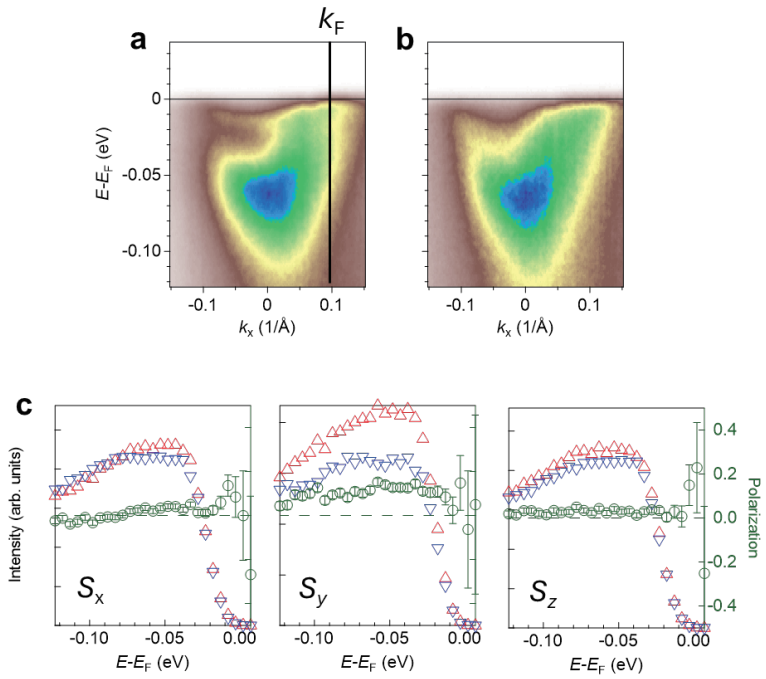

FIGURE 1. (a,b) ARPES dispersion across $\bar{\Gamma}$ before (a) and after (b) the spin polarization experiments, respectively. (c) Spin polarization data along *x*, *y*, and *z* directions. Note that *x* is parallel to k_x ($\bar{\Gamma}\bar{K}$) and *y* is parallel to k_y, and z is parallel to the surface normal.

REFERENCES

1. B.J. Kim et al., Nat. Phys. **2**, 397 (2006).
2. Z. Chen et al., Science **373**, 1235 (2021).
3. L. Ye et al., Nature **555**, 638 (2018).
4. H. Tanaka et al., Phys. Rev. B **101**, 161114(R) (2020).
5. S.A. Ekahana et al., Nature **627**, 67 (2024).
6. T. Iwata et al., Sci. Rep. **14**, 127 (2024).